

Effects of initial and boundary conditions on gravel-bed river morphology

Paudel, Sandesh; Singh, Umesh; Crosato, Alessandra; Franca, Mário J.

DOI

[10.1016/j.advwatres.2022.104256](https://doi.org/10.1016/j.advwatres.2022.104256)

Publication date

2022

Document Version

Final published version

Published in

Advances in Water Resources

Citation (APA)

Paudel, S., Singh, U., Crosato, A., & Franca, M. J. (2022). Effects of initial and boundary conditions on gravel-bed river morphology. *Advances in Water Resources*, 166, Article 104256. <https://doi.org/10.1016/j.advwatres.2022.104256>

Important note

To cite this publication, please use the final published version (if applicable). Please check the document version above.

Copyright

Other than for strictly personal use, it is not permitted to download, forward or distribute the text or part of it, without the consent of the author(s) and/or copyright holder(s), unless the work is under an open content license such as Creative Commons.

Takedown policy

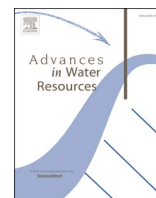
Please contact us and provide details if you believe this document breaches copyrights. We will remove access to the work immediately and investigate your claim.

Green Open Access added to TU Delft Institutional Repository

'You share, we take care!' - Taverne project

<https://www.openaccess.nl/en/you-share-we-take-care>

Otherwise as indicated in the copyright section: the publisher is the copyright holder of this work and the author uses the Dutch legislation to make this work public.



Effects of initial and boundary conditions on gravel-bed river morphology

Sandesh Paudel^{a,*}, Umesh Singh^{b,c}, Alessandra Crosato^{a,d}, Mário J. Franca^{a,d,e}

^a IHE Delft, Institute of Water Education, Department of Water Resources and Ecosystems, PO Box 3015, 2601, GA, Delft, the Netherlands

^b University of Trento, Department of Civil, Environmental and Mechanical Engineering, via Mesiano 77, 38123 Trento, Italy

^c Hydro Lab Pvt. Ltd, GPO Box No., 21093, Kathmandu, Nepal

^d Delft University of Technology, PO Box 5048, 2600, GA Delft, the Netherlands

^e Karlsruhe Institute of Technology, Engesserstraße 22, Geb. 10.83 - Raum 108, 76131 Karlsruhe, Germany

ARTICLE INFO

Keywords:

River channel formation
Gravel-bed rivers
Delft3D
Morphodynamic modeling
Initial conditions
Boundary conditions
Active width
Braid-belt extension

ABSTRACT

Assuming that the equilibrium geometry of river channels does not depend on their initial state but solely on boundary conditions, several formulas have been derived that relate the channel depth and width to the river bankfull discharge and bed material. However, due to the existence of a threshold for sediment motion and the strong non-linearity between sediment transport and flow rate, this assumption might not be generally valid for gravel-bed rivers. This research clarifies the role of the initial conditions, more specifically the initial channel width, on the geometry of gravel-bed rivers considering a variety of boundary conditions. The approach includes laboratory experiments and two-dimensional modeling, reproducing the evolution of alluvial channels with different starting widths, discharge regimes and sediment input rates. The experiments represent the Arc River (France). Thus, the characteristics of this river were used in the numerical model to obtain a realistic virtual case complementing the experiments. Different boundary and starting conditions resulted in either braided or single-thread channels. We found that the initial width strongly influences the evolution process and leaves a footprint on the river braid-belt extension. The active width of braided systems and the width of single-thread channels do not depend on the starting condition. They depend on sediment input rather than on discharge variability. Different initial widths result in different final bed levels. This indicates that the initial channel width may affect the degree of channel incision or aggradation. The results of this study justify the use of equilibrium formulas for single-thread rivers.

1. Introduction

Stable channels, having reach-averaged geometry that can be considered constant, belong to river reaches in morphodynamic equilibrium. The geometry of stable river channels has been described using the regime theory (Kennedy, 1895; Lacey, 1930; Leopold and Maddock, 1953; Parker et al., 2007), extremal hypothesis (Griffiths, 1984; Singh, 2003) and mechanistic approaches (Parker, 1978b). Several empirical relations have been formulated to determine the reach-averaged channel width and depth as a function of bankfull discharge (Leopold and Maddock, 1953; Williams, 1978; Parker, 1979; Emmett and Wolman, 2001) or as the formative discharge having a certain return time, normally 1.5 to 2 years (e.g. Vargas-Luna et al., 2019). Some formulas also include a dependency on sediment size and other physical features, such as riparian vegetation characteristics (e.g. Millar, 2005). Bray (1982), Garde et al. (2001), Millar (2005), Parker et al. (2007) and Kaless et al.

(2014) derived formulas for gravel-bed rivers, (Wilkerson and Parker, 2011) for sand-bed rivers, whereas Eaton and Church (2007) and Booker (2010) for both gravel-bed and sand-bed rivers, among others. A review is presented by Gleason (2015).

By relating the equilibrium channel geometry to discharge and other river characteristics, these formulas assume that the equilibrium channel configuration solely depends on boundary conditions which means that it is unaffected by the conditions at the start of the morphological evolution. However, this might not be true, especially for gravel-bed rivers, due to the presence of a clear threshold between sediment motion and non-motion (Shields, 1936; Garcia, 2008), and to the strong non-linearity of bed-load as a function of flow velocity, particularly at the conditions close to initiation of motion (Meyer-Peter and Müller, 1948). Starting from a narrow rather than wide channel could thus result in a totally different morphological evolution and probably also in a different long-term river configuration. Different starting widths imply

* Corresponding author.

E-mail address: sandeshpoudel0@gmail.com (S. Paudel).

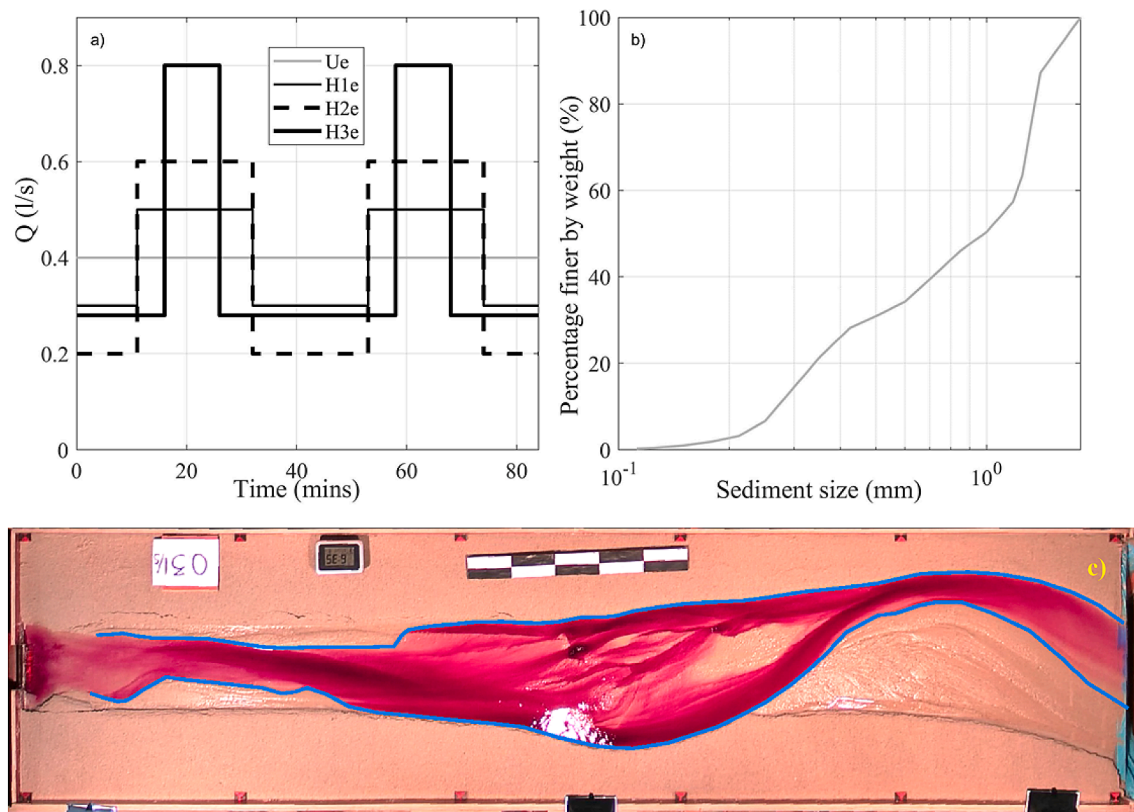


Fig. 1. a) Discharge hydrographs (mins = minutes), where subscript “e” stands for “experiment”. b) Grain size distribution. c) Channel in the laboratory flume. Coloured water highlights the wet surface. Flow is from right to left; the bar is 1 m long. The blue line indicates wet channel margins. (For interpretation of the references to colour in this figure legend, the reader is referred to the web version of this article.)

different water depths, flow distributions and sediment transport rates, affecting sediment outputs and thus also the sediment balance. The flow width-to-depth ratio is the major factor influencing the formation of bars, which in turn affect bank erosion and thus the channel width (Engelund, 1970; Crosato, 2009; Kleinhans et al., 2011). The initial channel width is therefore crucial in defining sediment transport and channel characteristics at the beginning of the morphological evolution, and might interact with the boundary conditions (water and sediment inputs and outputs) in a non-linear way, influencing the evolution path and the new equilibrium channel geometry (Blench, 1969; Mosselman, 2004).

Various works studied the effect of boundary conditions on the geometry of gravel-bed rivers. The importance of sediment supply was first realized by Schumm et al. (1972), who demonstrated that sediment feed reduction causes incision and affects the planform of laboratory channels. This was later confirmed by Wickert et al. (2013), Pfeiffer et al. (2017), Métivier et al. (2017) and Vargas-Luna et al. (2019). The effect of discharge was studied by Parker et al. (2003), Van De Lageweg et al. (2013), Blom et al. (2017), Schuurman et al. (2018) and Vargas-Luna et al. (2019) who emphasized the role of flow variability for the width evolution of gravel bed river system.

Works dealing with the effects of initial conditions are relatively less. Some work deals with tidal embayment (e.g. Van Maanen et al. 2013). In the case of rivers, Stecca et al. (2022) studied the role of initial bed perturbations on the distribution of channels and shoals in braided systems. However, the effect of initial conditions on reach-scale river geometry has not been analysed yet, whereas it could be significant for gravel-bed rivers. It is thus not clear whether gravel-bed rivers retain the footprint of their starting conditions in their morphology. In such a case, the formulas derived to assess the bankfull width and depth of stable gravel-bed channels may present important limitations.

This study analyses the evolution of un-vegetated gravel-bed river

systems towards equilibrium, departing from different channel widths in combination with different flow regimes and sediment input rates. The analysis focuses on the evolution of the reach-averaged channel width and bed level, as well as the river planform. The work includes a set of laboratory experiments and the simulation of several scenarios with a two-dimensional (2D) morphodynamic model developed using the open-source Delft3D code. The model reproduces the morphodynamic behavior of a realistic virtual gravel-bed river, derived by upscaling the experimental channels. The larger freedom that numerical models offer has allowed complementing the experiments by including additional scenarios and expanding the domain, considering, for instance, different sediment characteristics and longer time of evolution.

2. Materials and methods

2.1. Laboratory experiments

Six sets of laboratory experiments were conducted, whose layouts and test duration were designed to specifically study the evolution of initially straight channels towards morphodynamic equilibrium, starting from different widths, with several discharge regimes and sediment input rates (Singh, 2015). Attention was paid in producing the typical sediment mobility of gravel-bed rivers by selecting sediment and flow characteristics through a number of preliminary tests. The experiments were carried out in the Laboratory of Fluid Mechanics of the Delft University of Technology in a 5 m long, 1.24 m wide and 0.4 m deep flume. Water was recirculated from outlet to the inlet of the flume, whereas sediment was fed at the inlet at constant rates.

The flume was filled with non-uniform sand having median grain size, D_{50} , equal to 1 mm (Fig. 1b) and a straight rectangular channel, 4 cm deep with longitudinal slope of 1% and width of 4, 10, 25 or 40 cm, was excavated in the middle of the flume before the start of each test.

Table 1
Initial and boundary conditions of the experimental tests.

SN	Experiment scenario	Discharge regime	Sediment input rate	Initial width (m)
1	Ue	Constant	None	0.04, 0.1, 0.25, 0.4
2	H1e	Variable	None	0.1, 0.4
4	H2e	Variable	None	0.1, 0.4
5	H3e	Variable	None	0.1,0.4
6	Ue*	Constant	Constant: 90 g/min with the same granulometry as the alluvial corridor.	0.04, 0.1, 0.25, 0.4
7	H1e*	Variable	Constant: 90 g/min with the same granulometry as the alluvial corridor	0.1,0.4
8	H2e*	Variable	Constant: 90 g/min with the same granulometry as the alluvial corridor	0.1,0.4
9	H3e*	Variable	Constant: 90 g/min with the same granulometry as the alluvial corridor	0.1,0.4

Table 2
Scenarios simulated in numerical model.

SN	Model scenario	Discharge regime	Sediment input rate	Granulometry alluvial corridor	Initial width (m)
1	Um	Constant flow	None	Uniform	10, 30, 60, 100
2	Um ^{gr}	Constant flow	None	Graded	30, 100
3	H1m	Variable	None	Uniform	30, 100
4	H2m	Variable	None	Uniform	30, 100
5	Um*	Constant flow	Constant: 265 kg/s with the same sizes as alluvial corridor.	Uniform	10, 30, 60, 100
6	Um ^e	Constant flow	Variable: equal to local carrying capacity at the upstream boundary	Uniform	30, 60, 100
7	Um**	Constant flow	Constant: 265 kg/s and D ₅₀ of 2 cm: finer than the alluvial corridor	Uniform	30, 60, 100
8	H1m*	Variable	Constant: 265 kg/s with the same sizes as the alluvial corridor	Uniform	30 and 100
9	H2m*	Variable	Constant: 265 kg/s with the same sizes as the alluvial corridor	Uniform	30 and 100

The first two widths are considered narrow, resulting in initial conditions below the threshold for bar formation (Engelund 1970; Colombini et al., 1987; Tubino and Seminara, 1990; Crosato and Mosselman, 2009) and the last two are deemed wide, above the threshold of bar formation. The experiments followed the morphological adaptation of each channel as a response to different water and sediment inflow, focusing on reach-averaged width, bed level and planform. Four discharge hydrographs, including a constant flow (hydrograph Ue) and two sediment input regimes were implemented. Hydrographs H1e and H2e only differed in amplitude, whereas H3e, representing a rather intense but short flow, had high discharge of shorter duration. The same volume of water was discharged in the constant-flow and in the variable-flow tests through the duration of entire high-low flow cycles (Fig. 1a).

Video camera records taken from a nearly orthogonal position

allowed following the channel evolution. For the constant-flow tests, images were extracted from the videos at intervals of 30 min. For the variable-flow tests, images were extracted at the end of each low and high flow stages highlighting the contours of the wet channel by coloured water (Fig. 1c). These images were then used to quantify the temporal variation of reach averaged wet channel width (Section 2.3, Point 2), which was measured perpendicular to the channel centreline at intervals of 0.2 m in the central 3 m of the flume, thus removing the first and the last meter of flume close to the boundaries. Note that if the channel was braided the wet width also included some dry areas, corresponding to emerging bar tops (Fig. 1c) and for most cases, it covered the lateral extent of the area where the morphological process had occurred. Cross-section profiles were measured every 50 cm after 2 h and at the end of each test by laser scanning. This required to briefly stop the water flow after 2 h. Table 1 summarizes the initial and boundary conditions of each of the 20 tests that were carried out.

The experiments had duration of 7 h. The tests with variable discharge were carried out only for the initial widths of 10 and 40 cm. For these, the flow cycles shown in Fig. 1a were repeated 10 times. In most cases with sediment supply the channel widened very rapidly and soon touched the side walls of the flume, so that these tests had to be terminated earlier.

2.2. Numerical modeling

The numerical simulations were carried out on virtual channels having reach-scale characteristics similar to the Arc River in France (best resemblance to the experimental channels but not a scaled model), starting with different widths in combination with various inflow conditions. The objective was not to replicate or validate the experiments, but to complement them by extending the study at a real river scale, unaffected by scale issues. To design the virtual river, the average final configuration of the experimental channels (Ue Case) was upscaled and compared with rivers described in the literature (Appendix A).

2.2.1. Model description

The numerical simulations were carried out using the open-source software Delft3D (www.deltares.nl). This software allows performing morphodynamic computations by solving unsteady shallow water equations and sediment transport formulas to obtain bed-level changes, as well as changes in bed material characteristics (Singh et al., 2017). The models built for this research are based on a two-dimensional (2D) depth-averaged version of the basic equations, parameterizing the effects of 3D flow features. Models in this form have been successfully used to investigate morphological developments at a reach scale by Crosato and Saleh (2011), Schuurman et al. (2013), Singh et al. (2017), among others. A detailed description of the software and of the mathematical equations and corresponding numerical schemes, are provided by Deltares (2018).

2.2.2. Model setup

The spatial domain of the models was represented by a straight alluvial corridor 1500 m long and 300 or 400 m wide, depending on scenario, with initial longitudinal bed slope of 0.6% and sediment either composed of cobbles with uniform size or graded (Table 2). The granulometric curve of the sediment was obtained from the upscaled value of the experimental D₅₀, imposing a similar size distribution. The uniform sediment size coincided with the median diameter, D₅₀, of the graded sediment (Fig. 2b).

Additional 1000 m were added upstream and downstream of the study reach to minimize numerical error propagation from the boundaries, resulting in a 3500 m long model domain that was discretized in a rectangular computational grid having cell size of 5 m × 2.5 m (L × W). The grid was finer in transverse direction to better represent bank erosion (Williams et al., 2016). A trapezoidal-shaped, straight, 6 m deep initial channel with a flatbed was carved in the middle of the alluvial

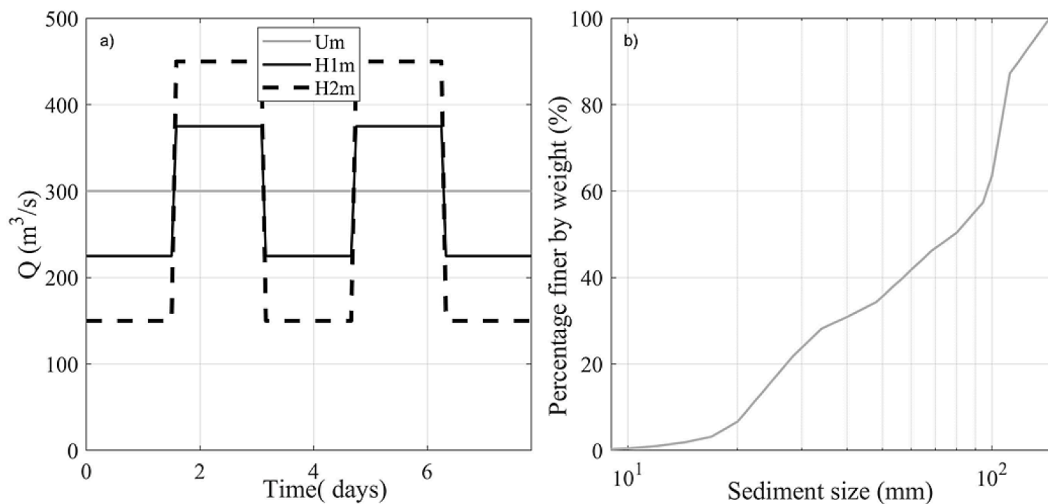


Fig. 2. Flow and sediment implemented in numerical model (a) Flow hydrographs: U_m , $H1_m$ and $H2_m$, where subscript “m” stands for “model”. (b) Granulometric curve of the virtual river bed (D_{50} , 8 cm) and alluvial corridor for the graded sediment scenarios.

corridor with side slope of 1V:1.67H. The average bottom width of the excavated channel varied according to scenario.

Model parameters were selected to best represent the trends and processes observed in the experiments, some through several sensitivity runs performed on a virtual channel (U_m -30), whereas some using typical suitable values for modeling rivers. The results of the sensitivity runs are presented in Appendix B.

To parameterize the flow resistance due to 3D-turbulence and horizontal motion, the eddy viscosity (V_h) was assigned the value of 0.1 m²/s, whereas sediment transport was simulated using the formula of Wong and Parker (2006), provided in Eq. (1).

$$q_s = 4.93 \sqrt{\Delta g (D_{50})^3} (\theta - \theta_{cr})^{1.6} \quad (1)$$

where, q_s represents volume rate of total bed-load transport per unit width without pores (m²/s), Δ represents the submerged specific gravity of sediment (-), g is the acceleration due to gravity (m²/s), D_{50} the median sediment size (m), θ the Shields parameter (-), with θ_{cr} being the critical shields parameter taken as 0.047.

In general, the direction of bed load doesn't coincide with the computed direction of depth-averaged flow velocity, because of the effects of gravity on bed slopes, commonly known as the bed-slope effect (Baar et al., 2019). In this study, Bagnold's (1966) was used to model the effects of longitudinal bed slope and the formulation of Ikeda (1982), as in van Rijn (1993), was used to model the effects of transverse bed slope (Eq. (2)):

$$q_n = |q_s| A_{bn} \sqrt{\frac{\theta_{cr}}{\theta}} \frac{\partial z_b}{\partial n} \quad (2)$$

where, q_n is the additional bed load transport vector in n direction due to gravity on transverse bed slope (m²/s, per unit width), q_s is the magnitude of the bed load transport vector in s direction adjusted for longitudinal bed slope only (m²/s), A_{bn} is a calibration coefficient, z_b is the bed level (m) and n is the transverse coordinate, perpendicular to the coordinate s (m).

The sediment transport direction is also affected by the spiral flow that develops in river bends, which tends to move the sediment particles towards the inner bend, opposite to the bed slope effect which pushes the sediment particles towards the outer-bend towards the pool (Schuurman et al., 2013). To parameterize the effects of spiral flow, this study adopted the formulation by Struiksmma et al. (1985).

The bed level changes were computed according to Exner's principle, i.e., assuming that the sediment transport immediately adapts to

changes in flow velocity, approach that is valid for bed-load dominated channels, typical of gravel-bed rivers. Bank erosion was modeled through the dry-cell/wet-cell algorithm available in Delft-3D redistributing the near-bank bed erosion. Based on the value imposed to a specific coefficient (0.8 in our case), the algorithm establishes the portion of bed erosion that is computed for a wet cell at the channel margin to be assigned to the adjacent dry cell (bank). This algorithm somehow reflects the physical process that near-bank bed erosion increases bank instability. In the model, wet and dry cells are identified based on a threshold water depth, which for this study was set equal to 10 cm. Such scheme for bank erosion has been successfully implemented in Schuurman et al. (2013), Williams et al. (2016) among many others. For the bed roughness, the Manning coefficient of 0.045 m^{-1/3} s ensured a Chezy roughness coefficient ranging between 20 and 30 m^{1/2}/s, in agreement with both the experimental channels and the Arc River (Jaballh et al., 2015).

The hydrodynamic time-step for the computations was 1.2 s, ensuring the stability of the model. In Delft 3D, the morphological changes can be accelerated by means of a specified factor (Morfac) to save computation time (Roelvink, 2006). For the constant discharge scenarios, a Morfac of 5 was used after ensuring that it does not significantly alter the morphological process (Appendix B). So, for these cases, a simulation of 10 days represents the morphological development of 50 computational days.

For the scenario with graded sediment, the granulometric curve (Fig. 2b) was divided in three equal fractions in terms of volume. Delft3D calculates the mean sediment diameter of each fraction and applies the prescribed sediment transport formula separately. The sediment continuity model proposed by Hirano (1971) was applied, dividing the bed in active and substrate layers of thickness 0.5 m and 1.87 m respectively. Following Singh et al. (2017), to mimic the hiding and exposure phenomenon, the models used the formulation of Parker et al. (1982), where a correction factor applied to the sediment transport formula increases the critical Shield number of the finer sediment fractions, reducing their entrainment rates (hiding), and decreases the one of the coarser fractions, increasing their entrainment rates (exposure).

The total duration of the simulations was selected based on pre-runs with the goal of achieving stable channels. For the cases without sediment feed, ending up as single-thread channels, the width of the channels presented very small changes after 50 days. However, at that point the average sediment transport and the bed slope were still decreasing at a consistent rate, but their changes became negligible after 70 days. For the cases with sediment feed, ending up as braided channels, the

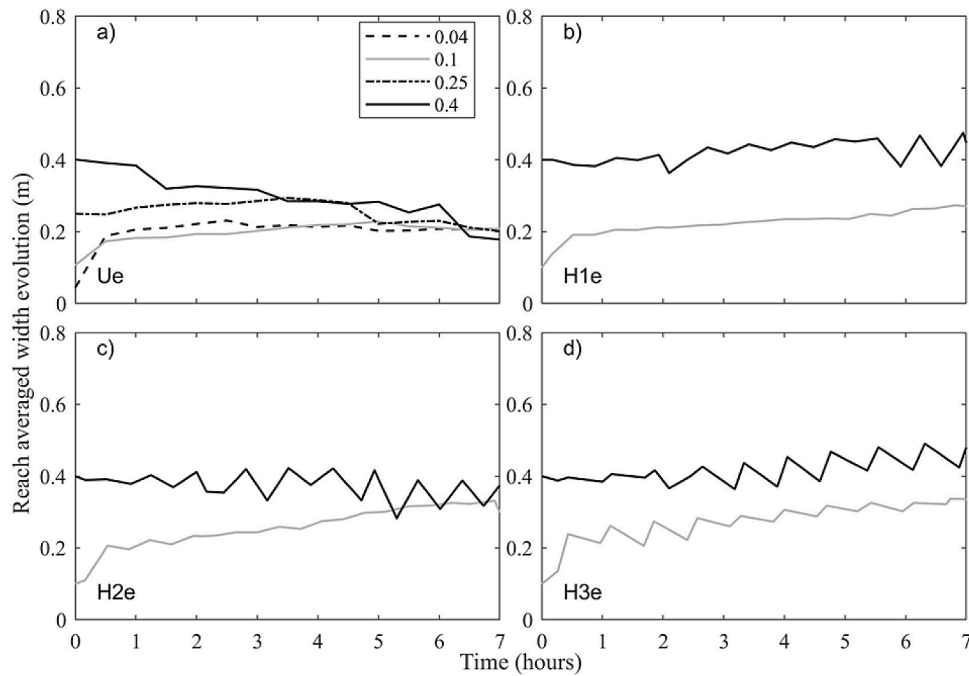


Fig. 3. Reach-averaged wet width evolution of the experimental channels without sediment feed, starting with different widths. a) Constant flow (Ue); b) Variable flow hydrograph H1e; c) Variable flow hydrograph H2e); d) Variable flow hydrograph H3e (hydrographs are shown in Fig. 1a).

duration of the computations had to be increased to 100 days. At that point, the average sediment transport of the reach had achieved a dynamic equilibrium, fluctuating around the input value. Note that in all cases the computational days cannot be linked to the real river time, considering that the value of the model discharges corresponds to short-duration high flows, not selected on the basis of Arc River's statistics. This shortcoming is considered acceptable because the focus of the work is to assess whether the configuration of stable gravel-bed rivers depends on initial conditions and not the temporal scales.

2.2.3. Model scenarios

Model scenarios were formulated with difference combination of starting widths and upstream boundary conditions (Table 2). For the upstream hydrodynamic boundary condition, three idealized hydrographs (Fig. 2a) were formulated, each one differing in amplitude but with the same duration and total volume of water inflow. The sediment input from upstream was either constant, nil, or equilibrium amount of bed load, with either the same size as the material forming the virtual channel and gravel plain, or with a smaller size. The downstream boundary conditions were a constant water level, derived for the initial channel, and the sediment output, was computed at the end of the model domain.

The constant sediment feed rates in the model were proportional to the ones in the corresponding experiments, derived using the relation presented in Eq. (3).

$$\frac{S_e}{T_e} = \frac{S_m}{T_m} \quad (3)$$

Where, S represents the sediment feed at the upstream boundary and T represents the sediment transport capacity of the narrowest initial channel, computed using Eq. (1) (subscript e means experiment and m is for model).

For the equilibrium sediment input, the bed load rate was equal to the transport capacity of the flow at the upstream boundary, calculated by the model at the upstream boundary based on the prescribed sediment transport formula (Eq. (1)).

The values of initial width to be imposed to the virtual channels were

derived based on geometric proportionality between experimental and virtual channels. The ratio between the average final width for the scenario Ue (i.e. 0.2 m) and the respective initial widths of the experimental channels was applied to the width of the River Arc, downstream reach where the river due to upstream damming has a strongly reduced bedload input (Jaballah et al., 2015). Similar to the experiments, the widths of 10 m and 30 m represented narrow initial channels, i.e. below the threshold for bar formation, while the initial widths of 60 m and 100 m represent the wide initial channels.

2.2.4. Analysis of the results

For gravel-bed river systems, Bertoldi et al. (2009) indicate three different widths, which was the basis of our analysis:

1. The *braid-belt extension*, being the transverse extension of the morphologically active area (Howard, 1996; Limaye, 2020). This is here taken as the lateral extent of the area in which the morphological changes have occurred.
2. The *wet river width*, defined as the lateral extent of the water surface at the bankfull condition (Parker et al., 2007) or at another defined discharge, which includes also emerging areas in between.
3. The *active channel width*, defined as the width of the portion of channel contributing to bed-load transport. This could not be measured in the laboratory channels.

For the study reach, excluding the first and last 1000 m of the model domain, widths were computed at each cross-section (5 m apart) and averaged to obtain reach averaged width. Width and bed adaptation interact and influence each other during channel evolution, so the evolution of the virtual channels was also analyzed as a combination of relative changes in average width and bed level showing four distinct phases: Aggradation/Widening, Aggradation/Narrowing, Incision/Narrowing, and Incision/Widening. The relative change in average width was computed as the difference between reach averaged evolved and initial width. The change in average bed level with respect to initial value at each cross-section was averaged to obtain relative change in bed level of the reach.

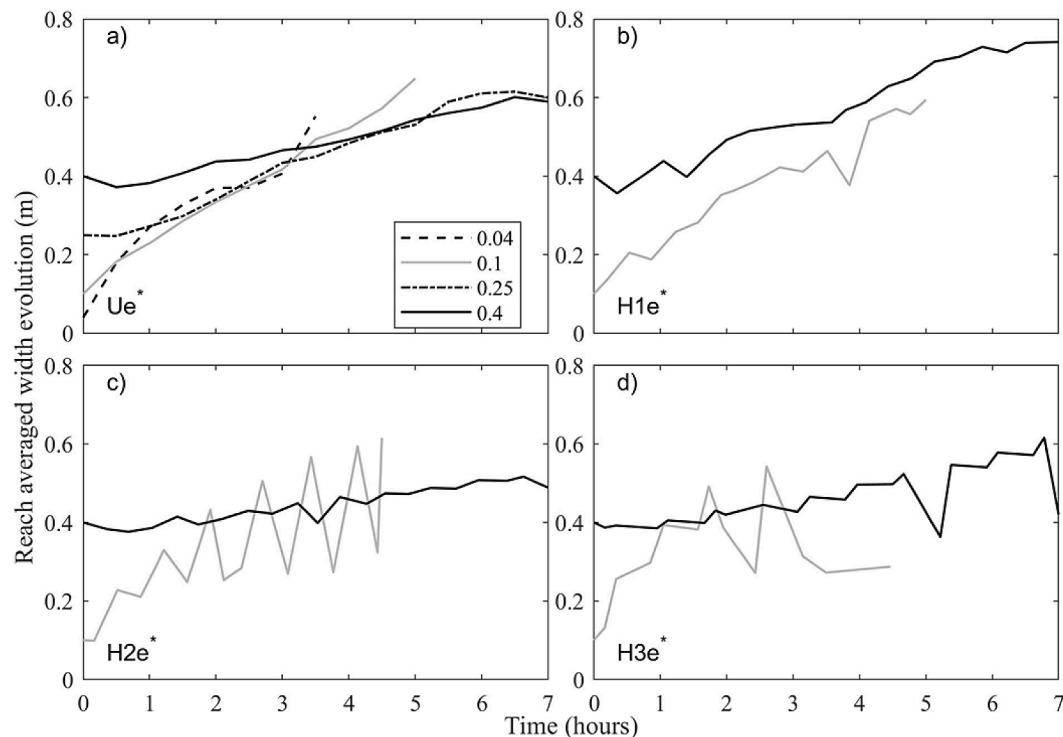


Fig. 4. Reach-averaged wet width evolution of the experimental channels with constant sediment feed of 90 g/minute, starting with different widths. a) Constant flow (Ue*); b) Variable flow hydrograph H1e*; c) Variable flow hydrograph H2e*); d) Variable flow hydrograph H3e*. Hydrographs are shown in Fig. 1a.

3. Results of the laboratory experiments

3.1. Without sediment input

Fig. 3 shows the width evolution of the channels having different discharge regimes (constant and variable with the same average and total flow volumes) without sediment feed at the upstream boundary.

Despite starting from different initial widths, all channels with constant flow (Ue scenarios, Table 1) evolved in single-thread systems ending up with a reach-averaged wet width of about 20 cm (Fig. 3a). However, the initially narrower (Ue-0.04 and Ue-0.1) and wider (Ue-0.25 and Ue-0.4) channels presented different evolution paths. The initially narrower channels started their evolution with rapid widening followed by widening at progressively smaller rates. Fast widening resulted in high sediment input (bank erosion products) to the channel and bed aggradation, followed by bed incision as the widening rate slowed down during the latest stage of evolution. Among the initially wider channels, Ue-0.25 presented slow channel widening and bed aggradation for the first 4.5 h. After achieving a width of about 30 cm, the channel started to narrow due to localized bed erosion. Ue-0.4 had initially a shallow flow distributed over the entire width and started producing some concentrated bed erosion which gradually progressed downstream. The eroded sediment initially was accumulated more downstream and was later partly removed by the flow. Channel narrowing by bed erosion was the dominant process towards the end of the experiment.

To study the effects of variable flow, the tests included the evolution of two channels with initial widths of 10 cm and 40 cm (Figs. 3b, 3c and 3d). Starting with a channel of 10 cm, the wet width development shows that the regimes with the highest flow peaks (H3e-0.1 and H2e-0.1) presented similar width oscillations (the wet width being a function of discharge) to end up with a similar width of about 35 cm (Fig. 3c and 3d gray lines), corresponding to a 75% increase compared to the constant-flow width. The variable discharge regime with the smallest peak (H1e) had initial evolution similar to the constant flow case Ue-0.1, but in H1e-

0.1 the channel continued to widen and finally resulted in a 25% wider channel, i.e. with a wet width of 25 cm instead of the 20 cm of the uniform flow scenarios (Figs. 3a and 3b gray lines).

With a starting width of 40 cm (Figs. 3b, 3c and 3d, black continuous lines), the H1e-0.4 and H3e-0.4 scenarios had similar evolution trends and ended up with 140% wider channels (48 cm) compared to the uniform flow scenarios (20 cm). These hydrographs had low flows with similar discharges (0.3 and 0.28 l/s), but with different duration: 20 and 28.5 min, respectively. They had strongly differed high-stage flows: 0.8 l/s (H3e) for a duration of 10 min, and 0.5 l/s (H1e) for a duration of 20 min. In the H2e-0.4 scenario, with smaller low discharge (0.2 l/s for 20 min) and an intermediate high discharge of 0.6 l/s for 20 min, instead, the channel slightly narrowed (from 40 to 38 cm), resulting in a 90% increase with respect to the final width of the uniform flow scenario (20 cm).

In general, all channels having the same flow regime without sediment feed show a tendency towards a similar width. If this is true, the final width would be independent from the initial one and only dependent on flow regime. Extrapolating the width evolution curves, we can observe that the final width of the channels would fall between 20 and 50 cm for all flow regimes.

In all tests, the high-stage flows occupied almost the entire width of the channel, whereas the low flows occupied only the deepest parts. The low flows of hydrographs H1e and H3e had enough intensity and duration to rework the bars that formed during the high discharge stages and to locally erode the banks. The next high discharge further reworked the bed and eroded the banks, resulting in channel widening. The higher flow peak with smaller duration of hydrograph H3e had effects that were similar to the lower, but longer, peak of hydrograph H1e. Instead, the lower discharge of hydrograph H2e was not sufficient to rework the bars formed during the high stage discharge and eroded the channel bed only in its deeper parts, further confining the low flow. The next high discharge reworked the bed across the entire width of the channel, but continued to erode also the deepest parts of the channel. Bed erosion started near the upstream boundary and advanced further downstream.

Table 3

Final wet width (single-thread channels) or braid-belt extension (braided channels), and final planform for different scenarios of numerical modeling.

Scenario	Sediment input	Granulometry alluvial corridor	Initial width (m)	Computational time (days)	Final wet width* or braid belt extension** (m)	Final planform
With sediment input smaller than the initial carrying capacity of the flow						
Um	No	Uniform	10	70	55.5*	Single-thread
			30	70	54.0*	
			60	70	48.4*	
			100	70	49.6*	
Um ^{8f}	No	Graded	30	70	32.5*	Single-thread
			100	70	44.2*	Single-thread, but braided in the last 400 m
H1m	No	Uniform	30	70	65.7/61.7*	Single-thread
			100	70	56.3/53.2*	
H2m	No	Uniform	30	70	69.4/64.3*	Single-thread
			100	70	59.7/54.7*	
Um**	Constant: 265 kg/s, but finer (2 cm) than alluvial corridor (8 cm)	Uniform	30	85	65.3*	Single-thread
			60	85	68.4*	
			100	85	61.8*	
With sediment input larger than or equal to the initial carrying capacity of the flow						
Um*	Constant: 265 kg/s, same size as alluvial corridor (8 cm)	Uniform	10	100	241.6**	Braided/overbank flow/ avulsions Braided
			30	100	159.4**	
			60	100	172.8**	
			100	100	204.3**	
Um ^e	Equilibrium sediment supply at the upstream boundary	Uniform	30	100	133.9**	Braided
			60	100	155.6**	
			100	100	196.9**	
H1m*	Constant: 265 kg/s, same size as alluvial corridor (8 cm)	Uniform	30	60	161.2**	Braided
			100	60	174.4**	
H2m*	Constant: 265 kg/s, same size as alluvial corridor (8 cm)	Uniform	30	60	175.5**	Braided
			100	60	180.3**	

Incision led to channel width reduction. These results indicate that the channel width depended on both high and low discharges, with the low flows having an important role in bar reworking and Thalweg deepening.

3.2. With constant sediment input

The results of the experimental tests with a constant feed of sediment having the same granulometry as the alluvial corridor are shown in Fig. 4. These tests produced much wider channels compared to the respective experiments without sediment feed (Fig. 3): final widths of approximately 50 to 75 cm compared to the 20 to 50 cm obtained without sediment feed.

The evolution of the channels with constant flow (Ue^* scenarios, Table 1) is shown in Fig. 4a. The initially wider channels seem to converge to the width of 60 cm. It is not possible to establish whether the initially narrower ones would also converge to the same width. These channels ($Ue^*-0.04$ and $Ue^*-0.1$) presented rapid widening and bed aggradation for the first 30 min. Bars started to appear after this period when the critical width-to-depth ratio for the formation of alternate bars exceeded. Bank erosion at pools produced sinuous and wider channels. As the channels continued to widen, complex mid-channel bars formed, a sign that at that point also the critical width-to-depth ratio for central bar formation had been reached. These tests had to be terminated well before reaching morphodynamic equilibrium, because the channel margins touched the sides of the flume. The initially wider channels ($Ue^*-0.25$ and $Ue^*-0.4$) started with higher width-to-depth ratios, so the first 30 min were already characterized by the development of alternate bars, followed by mid-channel bars. The growth of bars

enhanced bank erosion, resulting in wider multi-thread channels. Similar phenomena of channel widening were also observed by Ashmore (1982) in laboratory channels and by Jang & Shimizu (2005) in numerical simulations. As widening progressed, multiple bars were observed to migrate in downstream direction. Initially, $Ue^*-0.25$ presented higher widening rates than $Ue^*-0.4$, but after 4 h both channels evolved at similar widening rates, both resulting in reach-averaged widths of about 60 cm. Even though the final channel widths were similar, $Ue^*-0.25$ ended up with higher channel bed levels than $Ue^*-0.4$. In general, the channels having the same flow and sediment supply regime seem to converge towards a similar width, independently from their initial one, but the experiments were not long enough to exclude divergence in the final stages of morphological development. Variable discharges (Figs. 4b, 4c and 4d) produces wider channels than constant flow, but in general channel widening appears dominated by sediment input. However, many tests with variable discharge had to be terminated after 5 h because the channel touched the sides of the flume. For the same reason, the results of $H3e^*-0.1$ became not reliable after 3 h already.

4. Numerical model results

The evolution of the initially straight channels passed through various phases. The initial and final widths and the final planforms types are listed in Table 3. The initial and final planforms are presented in the supplementary materials.

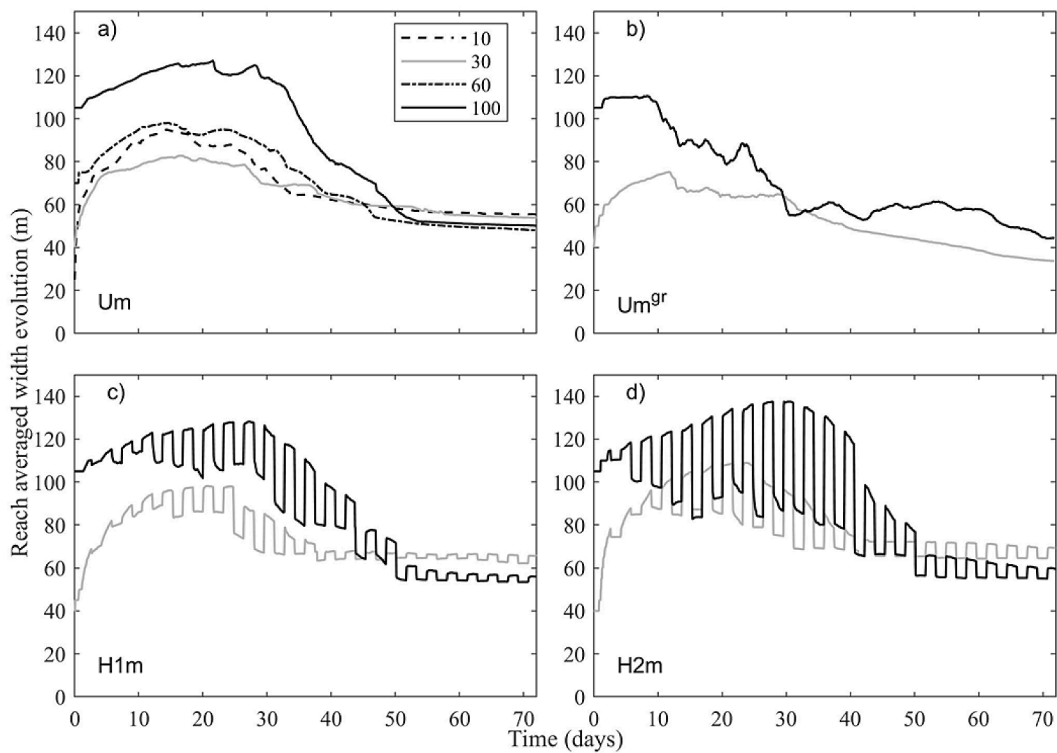


Fig. 5. Reach-averaged wet width evolution of channels without sediment input at the upstream boundary. Four different starting widths are considered: 10 m, 30 m, 60 m and 100 m. a) Constant flow (U_m) and uniform sediment. b) Constant flow (U_m^{gr}) and graded sediment. c) and d) Variable flow (H1m and H2m, respectively) and uniform sediment.

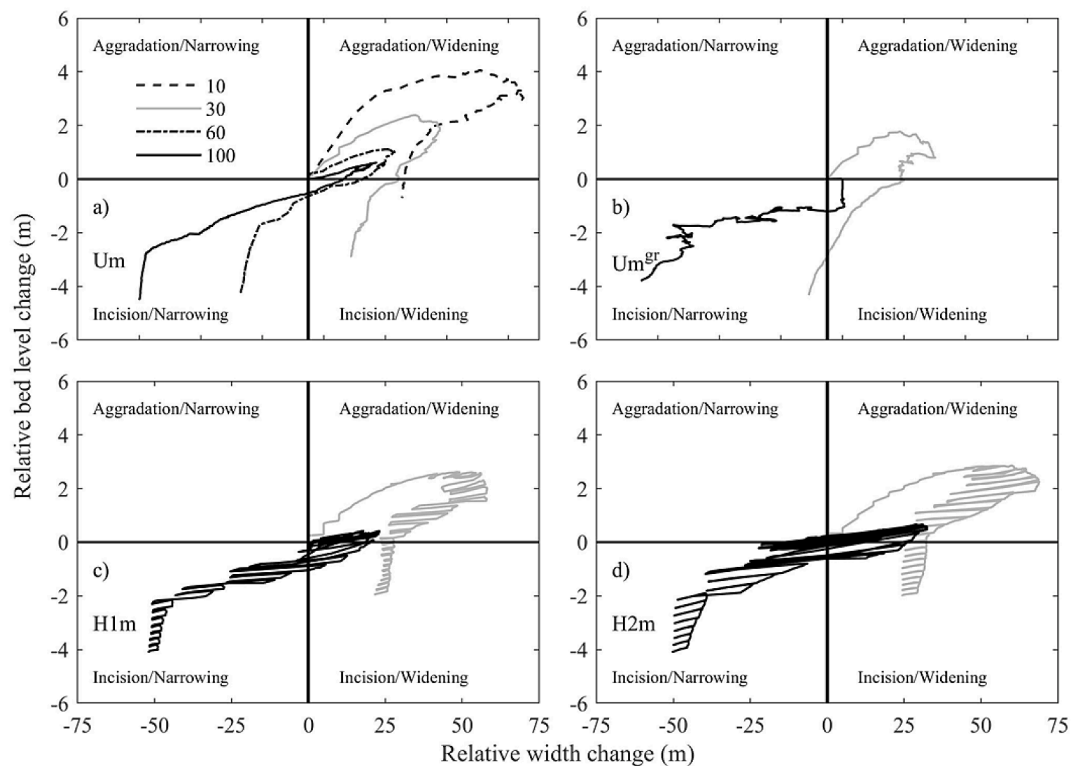


Fig. 6. Combined bed level and width evolution without sediment input at the upstream boundary. Four different starting widths are considered: 10 m, 30 m, 60 m and 100 m. a) Constant flow (U_m) and uniform sediment. b) Constant flow (U_m^{gr}) and graded sediment. c) and d) Variable flow (H1m and H2m, respectively) and uniform sediment.

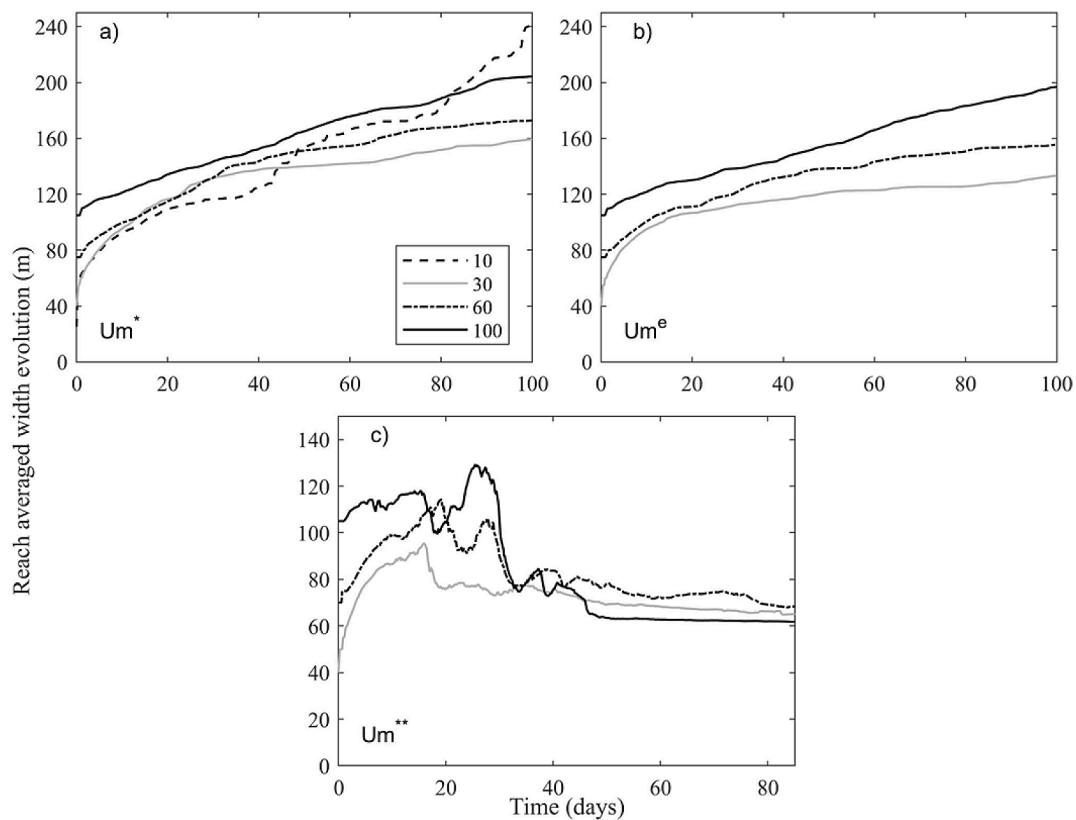


Fig. 7. Reach-averaged width evolution with constant flow and different sediment input regimes. Four different starting widths are considered: 10 m, 30 m, 60 m and 100 m. a) Evolution of braid-belt extension with constant sediment input rate (265 kg/s) having the same size (8 cm) as the channel bed and banks (U_m^*). b) Evolution of braid-belt extension with equilibrium sediment input computed as the local transport capacity of the flow at the boundary, having the same size (8 cm) as the channel bed and banks (U_m^e). c) Wet width evolution of the single-thread channels with a constant sediment input rate of 265 kg/s, having finer size (median diameter of 2 cm) than the channel bed and banks (U_m^{**}).

4.1. Without sediment input

Fig. 5 shows the reach-averaged width evolution of the channels that formed without sediment supply under different discharge regimes. All channels evolved in single-thread incised rivers with measurable differences in width, mainly depending on flow hydrograph. As expected, variable flows resulted in expansion and contraction of wet areas. The final width of the channels that formed under variable flow resulted systematically larger than with constant flow, with higher flow variability resulting in a wider channel, but only slightly. This was also observed by Vargas-Luna et al. (2019) in their laboratory experiments.

For uniform sediment and either constant (Fig. 5a) or variable discharge (Fig. 5c and 5d), the channels clearly widened during the initial phases of the model runs, and then narrowed, with the channels starting with the larger widths of 60 m and 100 m systematically became narrower than the channels that started with the smaller widths of 10 m and 30 m. Instead, with graded sediment and constant discharge (Fig. 5b), the larger initial channel ended up slightly wider than the channel that started with a smaller width. This could be due to bed armouring that limited the morphological process of incision/narrowing (see Fig. 6 and relative discussion). It should also be noticed that for the largest initial width sediment heterogeneity also resulted in the downstream part of the channel which was braided. However, in general, the final channels of the scenarios with graded sediment are narrower than with uniform sediment (compare Fig. 5a, 5b and Table 3).

Fig. 6 shows the combined width and bed level evolutions of the channels. If the bed sediment was uniform (Figs. 6a, 6c, and 6d), rapid widening governed the initial phase of the evolution of the channels that started with the smaller widths (10 m and 30 m). Distributed over an increasingly larger width, the flow gradually lost part of its sediment

carrying capacity, which, combined with a high sediment influx from the eroding banks, resulted in bed aggradation. When bank erosion stopped, due to lack of sediment input from upstream, the flow started eroding the channel bed, initiating an incision phase. For the initially wider channels, the aggradation/widening phase was much shorter, due to limited bank erosion. Again, when widening stopped, lack of sediment input caused incision and channel narrowing.

Fig. 6b shows the evolution of the channels with graded sediment and constant inflow. In this case, the aggradation/widening phase was much reduced compared to the scenarios with constant discharge and uniform sediment. The channel starting with the largest width ended up with a higher bed level (less incision) compared to the one with uniform sediment, which can be related to bed armouring due to sediment sorting (Sun et al., 2015). Instead, the channel starting with the smaller width ended up being narrower with a lower bed level. In this case, the high sediment carrying capacity of the flow concentrated in the narrower channel transported away the finer fraction rather quickly, deepening the channel in the areas with the highest flow rate. Here, the high velocity resulted in full mobility of the coarsest fractions, causing some extra channel incision. Regarding the effects of variable flow, for the same initial width, higher flow variability resulted in slightly higher widening and less incision.

4.2. With sediment input

Fig. 7 shows the reach-averaged width evolution for different sediment input regimes at the upstream boundary under constant discharge. The constant 265 kg/s and the equilibrium sediment input computed as the sediment transport capacity of the flow at the upstream boundary, with the same size as the channel bed and banks, were larger than the

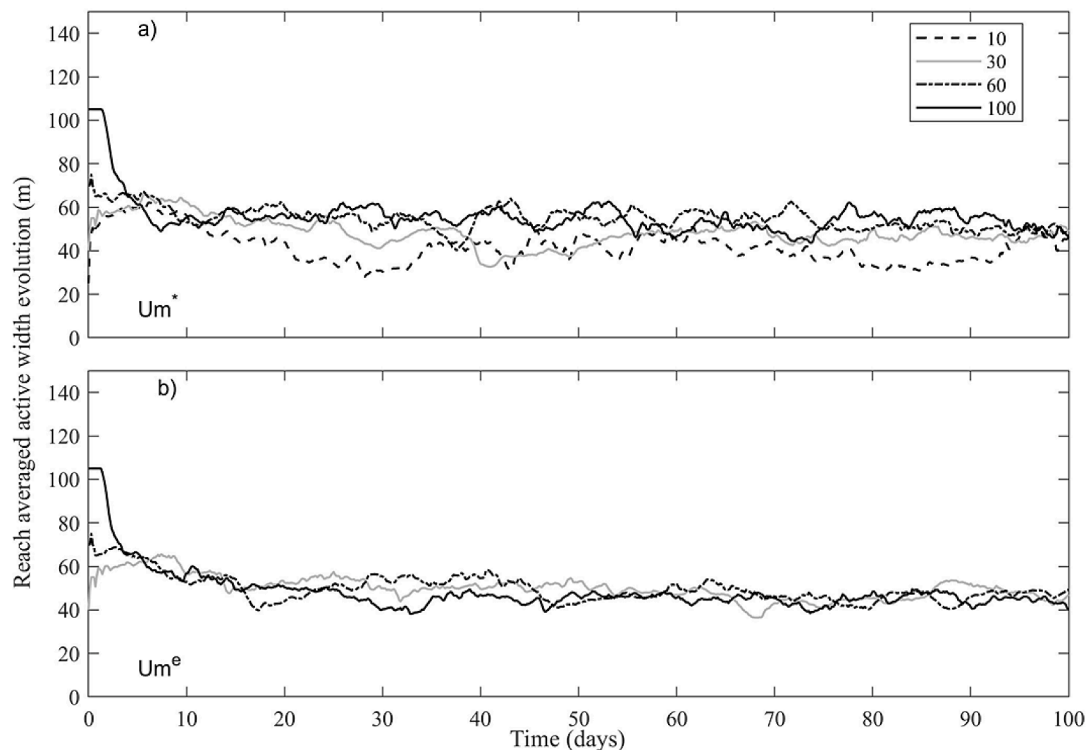


Fig. 8. Reach-averaged active width evolution. Four different starting widths are considered: 10 m, 30 m, 60 m and 100 m. a) Constant discharge and constant sediment input of 265 kg/s, having the same size as the channel bed and banks (U_m^*). b) Constant discharge and equilibrium sediment input, computed as the local transport capacity at the boundary, same size as channel bed and banks (U_m^e).

transport capacity of the flow further downstream (Fig. 7a and b). As a result, the channels widened significantly, with high bed aggradation leading to a braided planform. Instead, a constant input of 265 kg/s with finer sediment of uniform size (2 cm), was on average smaller than the sediment carrying capacity of the channels (Fig. 7c) and resulted in much narrower single-thread incised channels.

Figs. 7a and 7b show that different starting channel widths resulted in different braid-belt extensions. For a constant sediment input rate of 265 kg/s having the same size (8 cm) as the channel bed and banks (Fig. 7a), the narrowest initial channel produced the largest braid-belt (U_m^*-10). This channel started widening immediately with high bank erosion rates. The intense bed aggradation that followed initiated overbank flow and channel excavation through the alluvial corridor (after the 40th day) producing the widest braid belt. Similar morphological developments were observed by Schuurman et al. (2018). The other three starting widths (Fig. 7a and 7b) never presented overbank flow. Of these, the widest initial channels (U_m^*-100 and U_m^e-100) produced also the widest braid-belts. The equilibrium sediment supply, smaller than the constant input, produced narrower channels, in particular for the narrowest initial channel (Table 3). Constant input of finer sediment (Fig. 7c), smaller than the initial sediment capacity of the flow, resembles the case without sediment supply (Fig. 5a): after initial widening, all three channels became incised and single-thread with similar wet width.

The evolution of the active width of the braided channels, i.e., the width of the flow contributing to bedload transport, is shown in Fig. 8. Even though the channels produced different braid-belt extensions (Figs. 7a and 7b), the active widths tend to stabilize and converge to a similar value. Initial fluctuations were caused by the braiding activity of the channels.

Fig. 9 shows the combined width and bed evolution of the channels. If the sediment input is larger than the average transport capacity of the flow (Fig. 9a and 9b), the channels remain always in the aggradation/widening phase, with narrower channels experiencing more relative

width and bed level changes. The narrowest initial channel (U_m^*-10) presents the highest aggradation. The amount of relative aggradation and widening increases with sediment input (Fig. 9a and 9b). With finer sediment input, which was less than the average transport capacity of the channels, the combined evolution is similar to the case with no sediment supply with uniform sediment (Figs. 6a).

Fig. 10 shows the effects of variable discharge on the evolution of the reach-averaged braid-belt extension. The scenarios are distinguished by discharge regime ($H1m^*$ and $H2m^*$), but have the same constant sediment input of 265 kg/s (same size as alluvial corridor). These cases were simulated for a shorter period compared to the constant discharge cases, so they do not allow for a long-term analysis. Nevertheless, for both hydrographs the braid-belt extensions seem to converge irrespective of initial width, but they may diverge at a later stage, as in the cases with constant discharge (Fig. 7a and 7b).

5. Discussion

5.1. Controls of planform

Irrespective of boundary conditions, both the experimental and the virtual cases starting with the narrower widths shared similar trends at the start of their morphological evolution and so did the ones that started with the larger widths.

With or without sediment input, the initial phase of the narrower systems was characterized by high sediment transport capacity, due to flow concentration, and high bank erosion, resulting in rapid widening and channel aggradation due to the sediment input from bank erosion and (in certain cases) from the upstream boundary (Parker, 1978a). Migrating alternate bars appeared after reaching the critical width-to-depth ratio for bar formation (e.g. Engelund, 1970). Further channel widening led to multiple bar formation resulting in a braided system (Leopold and Wolman, 1957). The channel starting with the smallest width (10 m) experienced overbank flow because of excessive

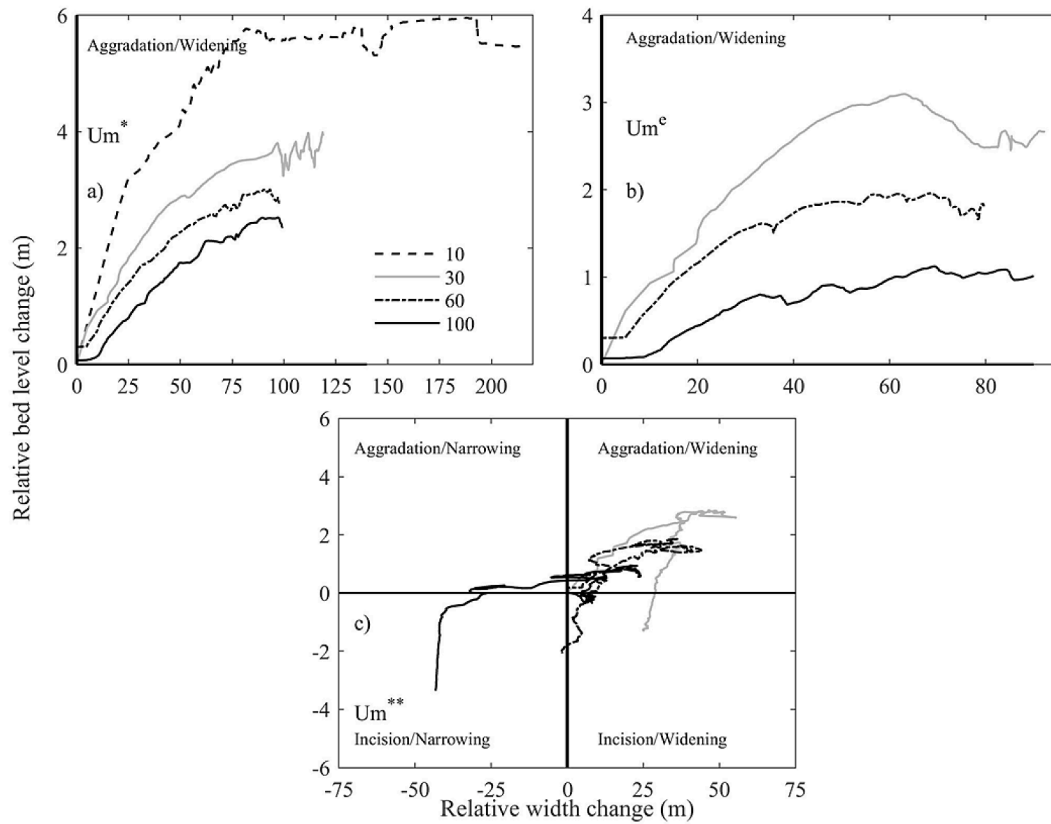


Fig. 9. Combined bed level and width evolution for different sediment input regimes and constant discharge. Four different starting widths are considered: 10 m, 30 m, 60 m and 100 m. a) Evolution of braid-belt extension with constant sediment input rate (265 kg/s) having the same size (8 cm) as the alluvial corridor (U_m^*). b) Evolution of braid-belt extension with equilibrium sediment input computed as the local transport capacity of the flow at the boundary, having the same size (8 cm) as the alluvial corridor (U_m^c). c) Wet width evolution of the single-thread channels with a constant sediment input rate of 265 kg/s, having finer size (median diameter of 2 cm) than the alluvial corridor (U_m^{**}).

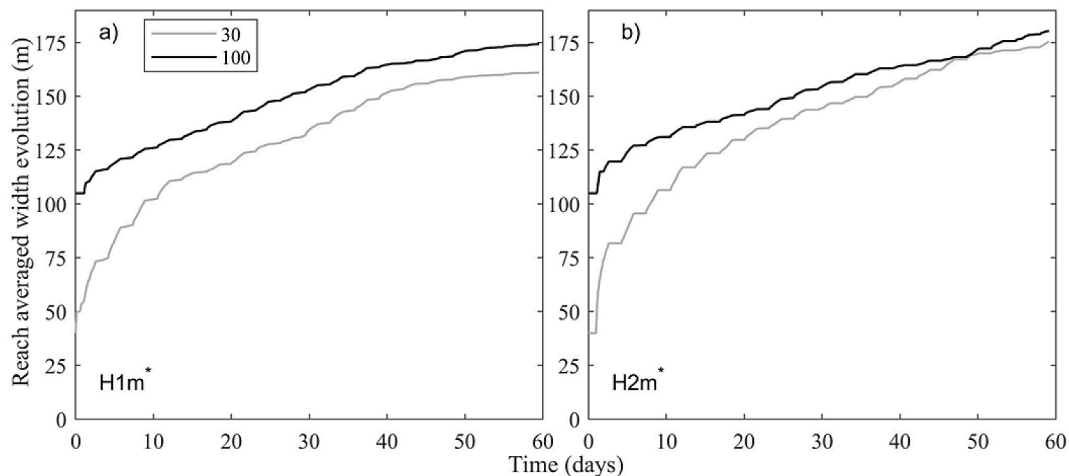


Fig. 10. Temporal evolution of reach-averaged braid-belt extension for the starting widths of 30 m and 100 m, variable flow and constant input of sediment (265 kg/s) having the same size as the alluvial corridor. a) Cyclic flow (H1m*) b) Cyclic flow (H2m*).

aggradation. For U_m-10 , it was in the form of sheet flow, but eventually the flow concentrated into a single channel (Pitlick et al., 2013), whereas for U_m^*-10 overbank flow interacted with the floodplain and produced chute-channels, which dominated the planform development (Schuurman et al 2018).

The initial phase of the wider channels was characterized by low-flow velocity not being enough to erode the banks. As a consequence, the channels did not widen much. Since the initial width-to-depth ratio

was already larger than the critical one, this phase was already characterized by bar development and the channels attained a braided planform relatively early. These observations confirm the results of previous studies (e.g. Murray and Paola, 1994; Bertoldi et al., 2009; Sun et al., 2015; Limaye, 2020).

For all cases, during the last phase, with further reduction of bank erosion and lateral sediment input, if the sediment input at the upstream boundary was smaller than the carrying capacity of the flow, bed erosion

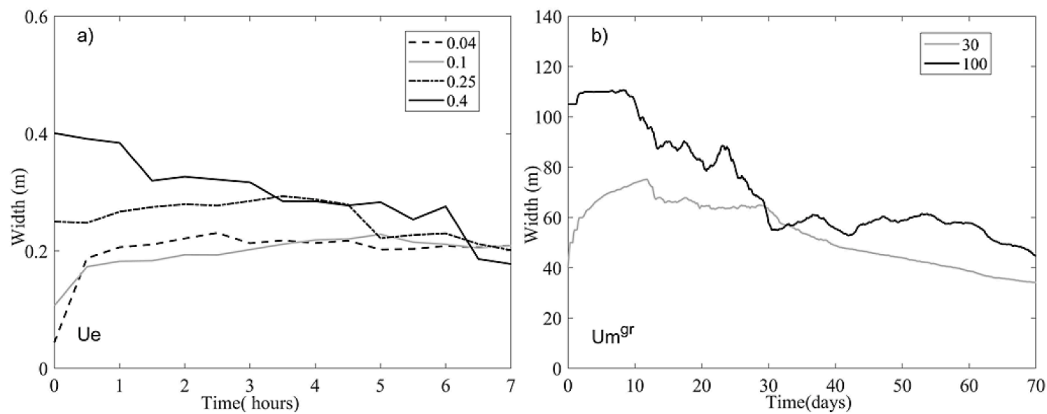


Fig. 11. Temporal evolution of reach-averaged wet width (vertical axis). a) Experimental channels (scenario with constant discharge and no sediment feed, From Fig. 3a). b) Virtual channels (scenario with constant discharge and no sediment feed, from Fig. 5b).

Table A.1

Comparison between the average final conditions of experimental tests 1 (Table 1), upscaled hypothetical channel and the conditions of real rivers described in the literature.

Characteristics	Unit	Experiment ¹ (Table 1)	Upscaled	River Arc ¹ downstream	River Arc ¹ upstream	River Severn ²	River Cecina ³
Location	–	–	–	France	France	England	Italy
Discharge (Q)	m ³ /s	4×10^{-4}	271.21	300	300	217	322
Width (w)	m	0.2	43	50	35	30	50
Depth (h)	m	0.0105	2.259	1.916	2.161	2.86	2.361
Average velocity	m/s	0.19	2.79	3.13	3.96	2.53	2.73
Longitudinal Bed slope (%)	–	0.663	0.663	0.6	1.1	0.14	0.21
Chezy coefficient (C)	m ^{1/2} /s	22.83	22.82	29.26	25.29	40.05	38.72
Froude number (F)	–	0.59	0.59	0.72	0.86	0.48	0.57
Shields Number (θ)	–	0.042	0.042	0.087	0.096	0.081	0.102
Median sediment size (D_{50})	mm	1	210	80	150	30	29.5
Width to depth ratio (w/h)	–	19.04	19.03	26.09	16.19	10.5	21.17
Bar mode (m)	–	1.3	1.3	1.66	1.2	0.48	1.06
2D flow adaptation length (λ_w)	m	0.28	59.96	83.26	72.8	233.47	180.41
2D water depth adaptation length (λ_s)	m	0.08	17.31	24.07	21.014	67.04	51.858
2D interaction parameter (IP)	–	0.289	0.289	0.289	0.289	0.287	0.287

¹ Arc River (Jaballah et al., 2015)

² Severn River (Singh, 2015)

³ Cecina River (Luppi et al., 2009; Teruggi and Rinaldi, 2009). * The variables/parameters of the real rivers are either from the respective pieces of literature or calculated with the relevant formulas with uniform flow assumption.

in the deepest parts of the channels propagated downstream, initiating channel narrowing, regardless of starting width. This resulted in the final transformation from a wide and braided system to narrow incised single-thread channel. Instead, if the sediment input was larger than the carrying capacity of the flow, the system remained braided and continued widening, but at an increasingly slower rate. Ideally, in the long run sediment mobility would reach the threshold value and channel widening would stop (Kleinhans et al., 2015b; Limaye, 2020).

Although the first phases of the morphological development were highly dependent on initial width, sediment supply seems to be dominant factor for the final river planform. This was already suggested by Schumm et al. (1972) and later by Métyvier et al. (2017), Pfeiffer et al. (2017) and Wickert et al. (2013).

5.2. Controls of lateral extension and bed level

Single-thread incised channels formed with sediment input rates smaller than the sediment transport capacity of the flow. For the same boundary conditions, these channels ended up with similar reach-averaged widths, with some differences, not retaining the memory of its starting width. Note that for the scenarios with no sediment input and constant discharge at the upstream boundary, the computed final width obtained starting from different values of channel width is similar to the actual width of the Arc River (50 m) as reported in Table A.1. This river

is dammed upstream and sediment input is occasional (Jaballah et al., 2015). With constant discharge, for the same starting widths, higher sediment inputs resulted in wider channels whereas variable flow also resulted in wider channels than constant flow (Vargas Luna et al. 2019), but the difference among the variable flow regimes was small (Table 3). Boundary conditions seems to govern the width of single thread channels and not the starting width.

Braided systems formed with sediment input rates that were larger than the sediment transport capacity of the flow. According to Bertoldi et al. (2009), Blom et al. (2017); Schuurman et al. (2018) and Limaye (2020), the braid-belt extension is primarily a function of discharge. Based on our results, we believe that it is also governed by the initial channel width and by the sediment input from upstream. We found that with a constant flow discharge, the final braid-belt extension increased if the initial width increased (Fig. 7, a and b). However, this is not valid for the smallest initial width, which produced the largest braid-belt of all. This was the only case that presented overbank flow excavating chute-channels through the floodplain. This process played a major role in the study of Schuurman (2018). With overbank flow, governed by peak discharges, it is possible that the braid-belt extension loses its dependency on initial width. The final braid belt for $Um^* - 30$ was 25.5 m wider than $Um^e - 30$, whereas for $Um^* - 100$ and $Um^e - 100$ it was only 7.4 m. Thus, a larger sediment feed produced a wider braid-belt but effected the narrow initial channel more.

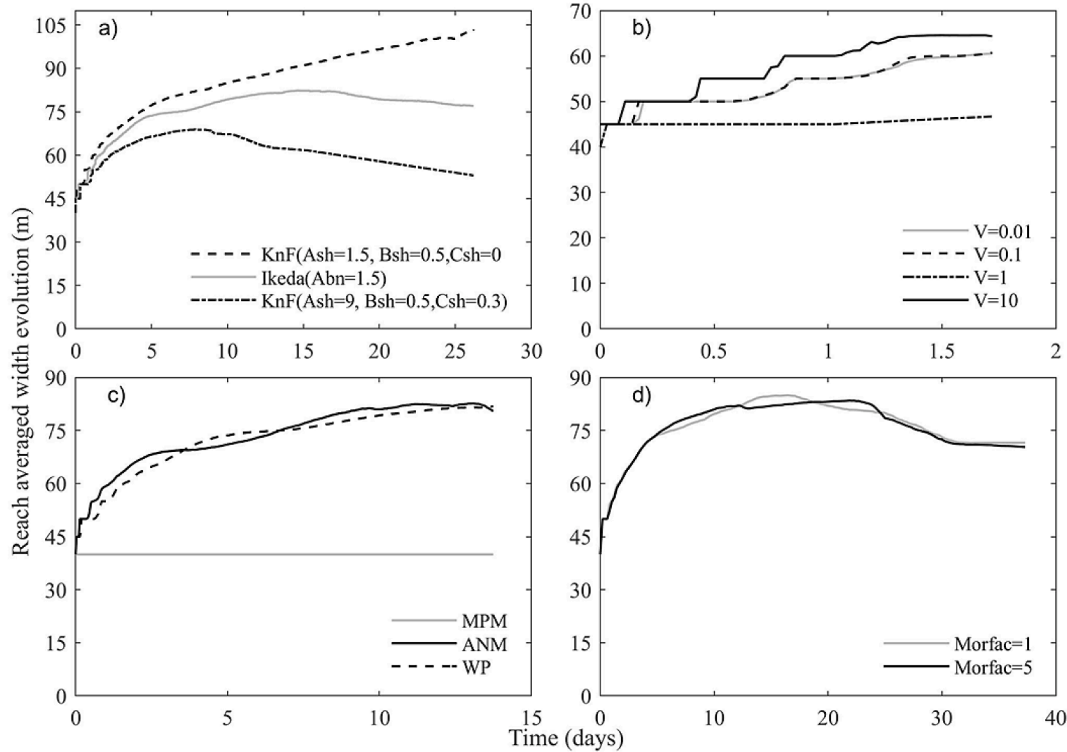


Fig. B.1. Results of sensitivity analysis of parameters; a) bed slope effects (Ash, Bsh, Csh are calibration parameter for KnF formulation), b) horizontal eddy viscosity, c) sediment transport formulas and d) morphological acceleration factor.

Simulation with variable flow and sediment feed were only ran for 60 days, shorter than constant discharge case, so it we could only analyze the medium-term evolution. The role of initial width is not as distinct as for constant discharge case at this point in evolution. Comparing the widths at the point where simulation for variable flow ended (i.e. 60th day), the widths of H1m*–30 and H2m*–30 are 19 m and 33 m wider than Um*–30. But widths of H1m*–100 and H2m*–100 are only 1 m and 5 m wider than Um*–100. Variable flow resulted in wider braid belt than with constant flow (Van De Lageweg et al. 2013; Blom et al., 2017; Schuurman et al. 2018) but the effect seems to be more for narrow initial channels. Note that these results are based on the effects of channel widening through bank erosion, since overbank flows did not occur for the 30 and 100 m initial channels.

About the active width, described in Section 2.3, Bertoldi et al. (2009) concluded that it is primarily a function of stream power (product of discharge and slope). This is supported by our model results, showing that the active width converged to a similar value for all the scenarios with the same boundary conditions, irrespective of initial conditions, even if the final braid-belt extension differed (Fig. 8). With the same constant discharge, the longitudinal slope of all our virtual channels increased from initial value of 0.6% to final values of around 0.7%. This indicates the modelled systems always had a similar stream power, and indeed resulted in a similar final active width.

The initial width is found to affect the final average bed level of the channel. Narrow initial widths resulted in higher final average bed levels than the wider initial widths, true for both aggrading and incising channels, which is primarily due to the high input of sediment from bank erosion (Figs. 6 and 9). For single thread incised channel, after intermediate widening and aggradation, all the channels started to incise from their aggraded bed. Narrow initial channels had higher aggradation before incision begun, so relative to the original bed level, they presented higher final bed level than initial wider ones. With graded bed material, sediment sorting limited incision of initial wider one while increasing that of narrower one, thus the channels ended up more or less at the same level. Also, variable flow presented higher relative widening

and aggradation thus having less channel incision than with a constant flow. In all cases, long-term progression of the morphological evolution would result in re-adaptation of the channel average bed level to the downstream boundary conditions (Jansen et al., 1979).

5.3. Combined experimental and numerical observations

The time scaling ratio suggested by Parker et al. (2003) and Pitlick et al. (2013) is:

$$\frac{T_e}{T_m} = \sqrt{L} \quad (4)$$

where T_e is the experiential time, T_m is the model time and L is the length scale (215 in this case).

Application of Eq. (4) indicates that 7 h in the experiments corresponded to 102 h (4 days) in the numerical simulations. The total duration of the model simulations was either 70 days or 100 days, which means that, in theory, the simulations covered a much longer adaptation period.

The experiments were carried out using non-uniform sand, and sediment sorting was indeed observed during the evolution of the channels. This means that the results of the laboratory study should be compared to the results of the graded-sediment scenarios of the numerical investigation, Um^{gr}, which were carried out for the initial widths of 30 and 100 m, with constant discharge and without sediment input (Fig. 11).

The evolution of the experimental and virtual channels followed similar trends (Fig. 11), but the experiment covered about half the evolution compared to the model. Both experimental and virtual channels tend to attain a similar final wet width, around 20 cm for the experimental channels and falling between 33 and 44 m for the virtual ones (Table 3). This gives confidence that the results of the numerical tests can indeed be used to complement the experimental ones, although in a qualitative way.

The experiments considered scenarios with variable discharge and sediment feeding, cases that were not reproduced with the numerical model for graded sediment. The results indicate that the widths tended to converge (Figs. 3 and 4). Without sediment feed, the final width appears governed by discharge variability, being about 0.2 m with constant flow (zero variability) and falling between 0.25 and 0.45 m for the variable discharge regimes (Figs. 3b, 3c and 3d). Considering that the experiments with variable discharge ended well before reaching morphodynamic equilibrium, if we qualitatively compare Fig. 4 to the model results of Fig. 5 (although with uniform sediment), we can observe that the discharge variability has a stronger effect during the evolution phase rather than on the final width. This means that even for the case without sediment feed, the effects of discharge variability are most probably less than the experiments would indicate. Moreover, from the experiments it seems that the final width would be only slightly larger with the high-peak regimes H2 and H3 than with the low-peak regime H1. In combination with sediment feed, the effects of discharge variability on wet width becomes visible only as an oscillation, being the final width close to 0.6 m with constant flow and between 0.4 and 0.75 m with all the variable flow regimes (Figs. 4b, 4c and 4d). With constant flow the introduction of sediment feed tripled the final channel width, from 0.2 to 0.6 m (compare Figs. 3a and 4a). In case of variable flow, the introduction of sediment feed less than doubled the channel width, i.e., from 0.25 to 0.45 m to 0.4–0.75 m. So, the effects of having variable flow instead of constant flow remain important: the peak flows rework bars and the low flows deepen the channels between the bars concentrating the sediment transport and reducing further channel widening. It is important to note that overbank flow did not occur during the experiments since the channels quickly widened through bank erosion so that the flow remained confined.

5.4. Equilibrium channel width predictors

If the sediment input rate is smaller than the initial sediment transport capacity of the flow, the results of this investigation suggest that the equilibrium channel width solely depends on boundary conditions. This is also true for the active width of the braided channels obtained with sediment supply larger than the initial transport capacity of the flow, but not for their braid-belt extension, which depends on intermediate morphological evolutions. This supports the use of equilibrium width predictors, considering that they are designed for applications on single-thread channels. With the purpose of analyzing the performance of predictors, the width of the experimental and virtual single-thread channels was computed using the approaches of Bray (1982), Parker et al. (2007) and (Millar, 2005). Note that these predictors consider the bankfull discharge as the formative one.

Bray (1982):

$$\left(\frac{W_{bf} S^{0.2}}{Q_{bf}^{0.4}}\right) = 4.73 \left(\frac{D_{50} S^{0.2}}{Q_{bf}^{0.4}}\right)^{-0.241}$$

$$S = 0.0449 \left(\frac{H_{bf}}{D_{50}}\right) - 0.945 \tag{5}$$

$$\frac{V}{\sqrt{g H_{bf} S}} = 1.97 S^{-0.256}$$

Parker et al. (2007):

$$W' = 4.63 Q'^{0.0667}, H' = 4.63 Q'^{-0.0004}, S = 4.63 Q'^{-0.344}$$

with

$$W' = \frac{g^{0.2} W_{bf}}{Q_{bf}^{0.4}}, H' = \frac{g^{0.2} H_{bf}}{Q_{bf}^{0.4}}, Q' = \frac{Q_{bf}}{D_{50}^2 \sqrt{g D_{50}}} \tag{6}$$

Millar (2005), without considering the effects of increased bank strength (no vegetation, no cohesion):

$$W' = 16.5 Q'^{0.7} S^{0.6}, H' = 0.125 Q'^{0.16} S^{-0.62}, \frac{W_{bf}}{H_{bf}} = 155 Q'^{0.53} S^{1.23} \tag{7}$$

with

$$W' = \frac{W_{bf}}{D_{50}}, Q' = \frac{Q_{bf}}{D_{50}^2 \sqrt{g D_{50} \Delta}}$$

Where Q_{bf} , H_{bf} and W_{bf} are the bankfull discharge (m^3/s), the bankfull water depth (m) and the bankfull channel width (m), respectively. Q' , H' , W' are dimensionless discharge, water depth and channel width, respectively, defined in different ways by Parker et al. (2007) and Millar (2005). S is the longitudinal channel slope, D_{50} is the median sediment diameter (m), g is the acceleration due to gravity (m/s^2), and V is the flow velocity (m/s).

Since flow variability is found to increase the channel width, the value of the discharge should be defined with care. For this, either the average discharge or the peak discharges, as suggested by Vargas-Luna et al. (2019) are used.

For the experimental channels, using the averaged discharge of 0.4 l/s, which is equal to the constant flow, the predictors of Bray (1982), Parker et al. (2007), and Millar (2005), estimate an equilibrium width of 0.29 m, 0.22 m and 0.29 m, respectively. Representing the bankfull discharge by the peak discharge, the estimated equilibrium widths become slightly larger: 0.33 m, 0.25 m, and 0.34 m for hydrograph H1e (Fig. 1); 0.36 m, 0.27 m, and 0.39 m for hydrograph H2e, and 0.41 m, 0.31 m, and 0.47 m for Hydrograph H3e, respectively. The predictions overestimate the widths obtained in the laboratory with constant flow and no sediment feed (20 cm), but underestimate the width of the channels with sediment feed and variable discharge (50–75 cm). The underestimations can be partly justified, since many experiments were terminated beforehand, at the start of their incision/narrowing phases, before the widths converged. Moreover, the experimental channels had unvegetated banks, whereas the predictors of Brey (1982) and Parker et al. (2007) were calibrated on existing rivers all presenting some type of riparian vegetation as well as some bank cohesion. Riparian vegetation controls the channel width in such a way that higher vegetation density results in narrower channels (e.g. Hey and Thorne, 1986).

For the virtual channels, using the average discharge of 300 m^3/s , Bray (1982), Parker et al. (2007) and Millar (2005) estimate equilibrium widths of 83 m, 59 m, and 104 m, respectively. Using the peak discharges, their estimates become 93 m and 102 m (Bray); 65 m and 71 m (Parker et al.); 121 m and 138 m (Millar), for the two hydrographs H1m and H2m, respectively. For comparison, the computed final width of the single-thread channels obtained with uniform sediment and input rates smaller than the initial transport capacity was 48–55 m with constant flow and 60–70 m with variable flow (Table 3). With graded sediment the computed channel width reduced to 33–44 m. With sediment supply larger than the initial transport capacity of the flow, all final channels were braided (Table 3), which means that the predictors cannot be applied for those cases. However, the active width of these channels was about 50 m. In general, all predictors tend to overestimate the width of the virtual channels. This could be attributed to the model limitations in representing bank erosion, particularly of incising channels (Section 5.5).

In any case, for both experimental and virtual channels, predicted and computed widths have the same order of magnitude.

5.5. Model limitations

Bank erosion is a complex geotechnical process affected by soil type, vegetation, and ground water table, among other, and plays an important role in channel widening. Delft3D uses a relatively simple algorithm for simulating bank erosion based on partial re-distribution of erosion from a wet cell to the adjacent dry cell. This somehow mimics the fact that toe bed erosion increases bank instability. A drawback of this scheme is that it does not work well as the water decreases and becomes

lower than the bank-top level during channel incision. So, even though the channel incised to a much deeper level the bank does retreat, i.e., it does not become wet and thus does not become a part of the channel in the model. These limitations in the bank erosion scheme might have affected the actual simulated morphological development.

The deviation of sediment transport direction due to gravity effects on a sloping bed is an important phenomenon shaping the two-dimensional riverbed topography. Considering a sloping near-bank river bed, if the effects are overestimated the result is excessive channel widening (due to excess of sediment displaced from the bank to the adjacent river bed) and an unrealistically flat bed-topography. Whereas if the value is underestimated, the results is unrealistic channel incision and lower channel widening. In our research, we opted for a medium bed slope effect, which gave sufficient representation of the process.

Considering these two factors affecting bank retreat, the computational algorithm for bank erosion and the gravity effect, we conclude that the quantitative results present inaccuracy leading to uncertainty. Nevertheless, we believe that the model captures well the morphological trends and is able to distinguish the simulated scenarios.

5.6. Applicability of the results

The results of this study present some practical aspects, such as the importance of initial width for the intermediate morphological evolutions of river channels. Most real rivers find themselves in this intermediate situation, since they are not in morphodynamic equilibrium.

Focusing on single-thread channels, the initially narrower ones experience an important widening/aggradation phase followed by incision with reduced width adjustments (slight widening or narrowing) before reaching their equilibrium configuration. The initially wider channels present a short phase with some widening and aggradation, but their main evolution trend is incision/narrowing. The final width of single-thread channels appears to depend on boundary conditions (water and sediment inflow) rather than on initial conditions.

Since the 1980s many rivers are now re-naturalized by removal of bank protection works, for instance in Europe and U.S.A. (e.g., [Kondolf et al., 2013](#); [Friedl et al., 2015](#) [Schmitt et al., 2018](#); [ONEMA, 2018](#); European center for River Restoration, www.ecrr.org; the River Restoration center, <http://www.therrc.co.uk/>). These rivers were once narrowed and at the moment of bank protection removal, find themselves in the situation of the initially narrower channels. Re-naturalized rivers show indeed an initial widening phase which might create worries to local managers due to the extent of widening and subsequent loss of valuable land (e.g., [Duró et al., 2020](#)). This study shows that after the initial widening phase accompanied by bed aggradation, there will be an incision phase with much reduced channel widening or even narrowing. Our study cannot give any indications on relative bed level changes, because both the experiments and the virtual rivers started with an imposed bed level which was not the result of morphological adaptation, i.e., the initial river channels were not in an equilibrium state. However, the results of our study indicate that the narrower initial channels end up with higher bed levels compared to the initially wider ones. All this is supported by theory ([Jansen et al., 1979](#); [Duró et al., 2016](#)).

Another application regards dammed rivers that after having their channels adapted to sediment shortage (normally by incision and narrowing) start to receive regular sediment by dam flushing ([Kondolf et al., 2014](#); [Dahal et al., 2021](#)). In this case, rivers are often in the situation of having a sediment input that is larger than the initial sediment transport capacity of their flow and at the same time have narrow channels. For these rivers, our study indicates an evolutionary trend towards braiding with the development of a braid-belt that is larger for the initially narrower channels and bed aggradation.

6. Conclusions

The work describes the morphological evolution of initial straight

channels, carved in cohesionless unvegetated gravel beds with different widths and sediment characteristics, under the forcing of combinations of flow regime and sediment input. The goal is to establish whether the reach-averaged width of gravel-bed rivers might depend on the conditions at the start of their morphological evolution. For braided systems, the analysis distinguishes the active channel width, where sediment transport occurs, from the braid-belt extension, indicating the width of the reworked floodplain. For single-thread channels, the analysis considers the wet width. The work includes a set of laboratory experiments and the simulation of several scenarios with a two-dimensional morphodynamic model, derived by upscaling the experiments, with the goal of replicating and extending the laboratory investigation, but at the scale of a real river.

Braided systems formed if the sediment supply was larger than the average transport capacity of the initial channel. Their braid-belt extension was found to depend on their initial width: the larger the initial channel the larger the braid-belt, but with one exception. The channel starting with the smallest width produced the largest braid-belt of all. This was the only case in which overbank flow occurred and reworked the floodplain. Chute channel formation rather than channel widening through bank erosion appears here to be the most important factor affecting the braid-belt extension. So, the dependency on initial width might only be valid in the absence of overbank flow and chute channel excavation. The results of both model and flume experiments show that the sediment supply governs the final planform of gravel-bed rivers. Higher sediment supply resulted in larger braid-belts, the initially narrow channels being more sensitive towards the amount of sediment supply than the initially wider ones. About the sediment transport width, the results of this work confirm [Bertoldi et al. \(2009\)](#) conclusion that the active width of braided systems is dominated by the stream power, i.e., discharge and slope.

Single-thread channels formed if the sediment supply at the upstream boundary was below the average transport capacity of the channels. For the same boundary conditions, these channels ended up with similar reach-averaged widths. Discharge variability seems to have a much stronger effect during the channel evolution phase than on final width. The application of width predictors to the experimental and virtual single-thread channels show that the ones proposed by [Bray \(1982\)](#), [Parker et al. \(2007\)](#) and [Millar \(2005\)](#) overestimate the width of the virtual channels and of the experimental channels with constant discharge and without sediment feed. Instead, they underestimate the width of the experimental channels with sediment feed and variable discharge. In any case, the predicted and measured/computed widths have the same order of magnitude and the differences can be explained by the experimental settings and model limitations. This work therefore supports the use of width predictors for single-thread gravel-bed rivers. The initial widths affected the final average bed levels (the narrower initial channels became on average higher), indicating that the initial channel width may affect, the degree of channel incision or aggradation. It is likely though that on the long-term the bed level of all the channels adjusts to the downstream boundary conditions.

The results of this work, showing how the river width evolves before reaching its final value can be useful for river restoration projects and major river interventions.

CRediT authorship contribution statement

Sandesh Paudel: Conceptualization, Methodology, Software, Formal analysis, Writing – original draft, Writing – review & editing. **Umesh Singh:** Conceptualization, Methodology, Investigation, Formal analysis, Writing – review & editing. **Alessandra Crosato:** Conceptualization, Methodology, Writing – original draft, Writing – review & editing, Supervision. **Mário J. Franca:** Writing – review & editing, Supervision.

Declaration of Competing Interest

The authors declare that they have no known competing financial interests or personal relationships that could have appeared to influence the work reported in this paper.

Acknowledgments

The first author was funded by the Orange Knowledge Program (OKP) of the Netherlands Government, reference CS-SA/MRA/ACAD 2018. The authors would like to express their gratitude to IHE Delft for facilitating the use of virtual computers (Surf Sara's HPC Cloud Service) for the purpose of carrying out the model runs. The laboratory experiments were carried out in the Laboratory of Fluid Mechanics of the Delft University of Technology (TU Delft) within the SMART Joint Doctorate (Science for the Management of Rivers and their Tidal systems) funded with the support of the Erasmus Mundus program of the European Union and managed by Prof. Guido Zolezzi, University of Trento (Italy). Thanks to Wim Uijttewaai for providing facilities for the experiments and Jairo Angel Escobar and Harmen Schölvink for helping to carry out the experiments. Finally, the authors wish to thank John Pitlick, University of Colorado, and Maarten Kleinhans, Utrecht University, who thoroughly reviewed our manuscript and, with very constructive comments, helped improving it.

Appendix A: Identifying representative rivers

Upscaling of the experiments allowed describing the type of rivers that was reproduced in the flume (e.g. Garcia, 2008). Establishing the characteristics of the hypothetical real river represented by the flume experiments was done on the average final configuration of the channels belonging to scenario Ue (Table 1). The artificially imposed starting width and straight alignment did not allow to do this in the design phase of the experiments.

Assuming turbulent flow, similar flow and sediment mobility are obtained if the Froude and the Shields numbers have the same values. Geometric similarity is necessary to well represent depth-dependent processes, like the deviation of sediment transport direction by transverse bed slope and bank erosion. In addition, imposing the same width-to-depth ratio is necessary to obtain a similar 2D morphodynamic behavior, since bar characteristics primarily depend on this ratio (Tubino and Seminara, 1990). As an alternative, similarity in 2D morphodynamic can be obtained by imposing the same value of the interaction parameter (Struiksma et al., 1985; Kleinhans et al., 2015a) or of the bar mode (Crosato and Mosselman, 2009), which are both dependent on width-to-depth ratio and sediment mobility.

The experiments were upscaled using the principles described above, imposing to the upscaled channel the same longitudinal slope, bed roughness, Froude and Shields numbers, interaction parameter and bar mode of the experiment and the geometric scale of 215 (chosen to represent a typical mountain river size), following the approach of Le et al. (2018). The obtained hypothetical river characteristics were then compared to the ones of existing river reaches reported in the literature (Table A.1) to establish the level of realism of the experiment and to select the most-resembling real river case for the setup of the morphodynamic model.

The downstream reach of the River Arc (France) described by Jaballah et al. (2015) is the real case with the highest resemblance to the upscaled experimental channel. Both have relatively steep bed slopes around 0.6%, but the Arc River has smaller median sediment size, although still in the range of cobbles. For both the upscaled channel and the Arc River, the Shields parameter falls between 0.01 and 0.2, which according to Garcia (2008) is typical of gravel-bed rivers at conditions close to initiation of sediment motion, or comparatively low mobility. The discharge of 300 m³/s, corresponding to a 10-year return-period flood of the Arc River, is comparable to the upscaled constant

discharge. This indicates that the constant-flow experiments represented rivers with continuous high flow conditions. The low-flow stages of the experiments with variable discharge represented medium stages of real rivers. In mountain rivers high discharges are responsible for most morphological changes (Vargas-Luna et al., 2019). However, our experiments have indicated that medium flow stages are important for Thalweg forming and bar reworking. Using relatively high discharges is therefore acceptable bearing in mind the scope of this investigation, which focuses on the long-term evolution of trends and processes governing the channel formation of gravel-bed rivers towards equilibrium, without considering the time scale for these changes to occur.

Appendix B: Sensitivity analyses

Several sensitivity runs were performed on the virtual channel of Um-30, to select the suitable model parameters. During the test, parameters of interest was varied by holding other parameters constant.

Two commonly used formulations in Delft3D to represent the transverse bed slope effect are; formulation of Ikeda (1982), as in van Rijn (1993), and the formulation of Koch & Flokstra's (1980) extended by Talmon et al. (1995), KnF. Fig. B.1a shows the comparison between these two formulations focusing on channel width evolution. Small transverse bed slope effect produced small bars, narrow channels with high incision and less channel widening, while high bed slope effect had the opposite effect with much higher channel widening (Schuurman et al. 2018), represented by two typical sets of parameters (Singh et al., 2017), with KnF formulation (Fig. B.1a). For our virtual channels, the parametrization with Ikeda formulation ($A_{bn} = 1.5$, default value in Delft 3D), seemed suitable with respect to the extent of channel widening and incision as compared to KnF formulation.

The default value of horizontal eddy viscosity (10 m²/s) did not satisfy the model stability criteria, as described in (Deltares, 2018), mainly due to the fine grid size of the models. The value of 1 m²/s, underestimated channel widening and sediment transport rates and resulted in an increase of flow velocity in shallow areas and a decrease in the deeper parts. The values of 0.1 m²/s and 0.01 m²/s resulted in similar acceptable velocity distributions and width development (Fig. B.1b). So, a value of 0.1 m²/s was chosen for the horizontal eddy viscosity.

The virtual river represented a gravel-bed river dominated by bed-load transport. Three sediment transport formulas, particularly suitable for the computation of coarse sand and gravel transport rates: Mayer-Peter & Muller (1948), MPM, Ashida and Michiue (1972), ANM, and Wong & Parker (2006), WP, were compared based on channel width evolution (Fig. B.1c). The formula by Wong & Parker (2006) (Eq. (1)) was the one that best represented the sediment transport in the experimental channel as well as in the River Arc. MPM produced no widening due to form factor which affects the sediment mobility (Schuurman et al., 2013); ANM and WP produced similar widening but ANM resulted in much higher incision.

Fig. B.1d compares the channel width evolution obtained using a morphological accelerator equal to 5 (Morfac = 5), a way to save computational time (Roelvink, 2006), and the channel width obtained without morphological accelerator (Morfac = 1). The results show that for the scenarios with constant discharge, the morphological development could be accelerated by a factor of 5 without losing important information. So, for these cases, a simulation of 10 days represents the morphological development of 50 computational days. With the selected set of parameters, the trends in morphological evolution of the virtual river were similar to the ones observed in the experimental channel and were used to set up the model.

Supplementary materials

Supplementary material associated with this article can be found, in the online version, at doi:10.1016/j.advwatres.2022.104256.

References

- Ashida, K., Michiue, M., 1972. Study on hydraulic resistance and sediment transport rate in alluvial stream. *Transactions, JSCE* 206, 55–69. <https://doi.org/10.2208/jsej1969.1972.206.59> (in Japanese).
- Ashmore, P.E., 1982. Laboratory modelling of gravel braided stream morphology. *Earth Surf. Process. Landforms* 7, 201–225. <https://doi.org/10.1002/esp.3290070301>.
- Baar, A., Albernaz, M.B., van Dijk, W., Kleinhans, M., 2019. Critical dependence of morphodynamic models of fluvial and tidal systems on empirical downslope sediment transport. *Nat. Commun.* 10 (1), 1–12. <https://doi.org/10.1038/s41467-019-12753-x>.
- Bagnold, R.A., 1966. An Approach to the Sediment Transport Problem from General Physics. US government Print Office. <https://doi.org/10.3133/pp4221>.
- Bertoldi, W., Zanoni, L., Tubino, M., 2009. Planform dynamics of braided streams. *Earth Surf. Process. Landforms* 34 (4), 547–557. <https://doi.org/10.1002/esp.1755>.
- Blench, T., 1969. *Mobile-bed Fluviology*. University of Alberta Press, Edmonton, Alberta, Canada.
- Blom, A., Arkesteijn, L., Chavarrías, V., Viparelli, E., 2017. The equilibrium alluvial river under variable flow and its channel-forming discharge. *J. Geophys. Res.* 122 (10), 1924–1948. <https://doi.org/10.1002/2017JF004213>.
- Booker, D.J., 2010. Predicting wet width in any river at any discharge. *Earth Surface Process. Landforms* 35 (7), 828–841. <https://doi.org/10.1002/esp.1981>.
- edited by Bray, D.J., 1982. Regime equations for gravel-bed rivers. In: Hey, R.D., Bathurst, J.C., Thorne, C.R. (Eds.), *Gravel-Bed Rivers*. John Wiley, Chichester, UK, pp. 517–542. edited by 517-542.
- Colombini, M., Seminara, G., Tubino, M., 1987. Finite-amplitude alternate bars. *J. Fluid Mech.* 181, 213–232. <https://doi.org/10.1017/S0022112087002064>.
- Crosato, A. (2009). Physical explanations of variations in river meander migration rates from model comparison. 34(15), 2078–2086. doi: <https://doi.org/10.1002/esp.1898>.
- Crosato, A., Mosselman, E., 2009. Simple physics-based predictor for the number of river bars and the transition between meandering and braiding. *Water Resour. Res.* <https://doi.org/10.1029/2008WR007242>. AGU, Vol. 45, article No W03424.
- Crosato, A., Saleh, M.S., 2011. Numerical study on the effects of floodplain vegetation on river planform style. *Earth Surf. Processes Landforms* 36 (6), 711–720. <https://doi.org/10.1002/esp.2088>.
- Dahal, S., Crosato, A., Omer, A.Y.A., Lee, A.A., 2021. Validation of model-based optimization of sediment releases by dam removal. *J. Water Resour. Plann. Manage.* 147 (7), 04021033 [https://doi.org/10.1061/\(ASCE\)WR.1943-5452.0001388](https://doi.org/10.1061/(ASCE)WR.1943-5452.0001388), 2021.
- Deltares. (2018). *Delft3D-FLOW user manual*.
- Duró, G., Crosato, A., Tassi, P., 2016. Numerical study on river bar response to spatial variations of channel width. *Adv. Water Resour.* 93 (A), 21–38. <https://doi.org/10.1016/j.advwatres.2015.10.003>.
- Duró, G., Crosato, A., Kleinhans, M.G., Winkels, T.G., Woolderink, H.A.G., Uijttewaal, W. S.J., 2020. Distinct patterns of bank erosion in a navigable regulated river. *Earth Surf. Processes Landforms*. <https://doi.org/10.1002/esp.4736>.
- Eaton, B.C., Church, M., 2007. Predicting downstream hydraulic geometry: a test of rational regime theory. *J. Geophys. Res.* 112 <https://doi.org/10.1029/2006JF000734>. F03025(F3).
- Emmett, W.W., Wolman, M.G., 2001. Effective discharge and gravel-bed rivers. *Earth Surf. Processes Landforms* 26 (13), 1369–1380. <https://doi.org/10.1002/esp.303>.
- Engelund, F., 1970. Instability of erodible beds. *J. Fluid Mech.* 42, 225–244. <https://doi.org/10.1017/S0022112070001210>.
- Friedl, F., Weitbrecht, V., Boes, R.M., 2015. The role of Bank Erosion in Restoration Works in Gravel-Bed Rivers. In: E-Proceedings of the 36th IAHR World Congress. 29 June-3 July 2015, The Hague, the Netherlands.
- García, M.H., 2008. Sediment transport and morphodynamics. *Sediment. Eng.* 21–163. <https://doi.org/10.1061/9780784408148.ch02>.
- Garde, R.J., Prakash, H., Arora, M., 2001. Hydraulic geometry and resistance of gravel-bed rivers. *ISH J. Hydraul. Eng.* 7 (2), 51–66. <https://doi.org/10.1080/09715010.2001.10514698>.
- Gleason, C.J., 2015. Hydraulic geometry of natural rivers: a review and future directions. *Progr. Phys. Geog. Earth Environ.* 39 (3), 337–360. <https://doi.org/10.1177/2F0309133314567584>.
- Griffiths, G.A., 1984. Extremal hypotheses for river regime: an illusion of progress. *Water Resour. Res.* 20 (1), 113–118. <https://doi.org/10.1029/WR020i001p00113>.
- Hey, R.D., Thorne, C.R., 1986. Stable channels with mobile gravel beds. *J. Hydraul. Eng.* 112, 671–689.
- Hirano, M. (1971). *River-bed degradation with armoring*. Paper presented at the Proceedings of the Japan society of civil engineers.
- Howard, A.D., 1966. Modelling channel evolution and floodplain morphology. In: Anderson, M.G., Walling, D.E., Bates, P.E. (Eds.), *Floodplain processes*. John Wiley and Sons, Ltd., Chichester, pp. 15–62.
- Ikeda, S., 1982. Incipient motion of sand particles on side slopes. *J. Hydraul. Div.* 108 (1), 95–114. <https://doi.org/10.1061/JYCEAJ.0005937>.
- Jaballah, M., Camenen, B., Pénard, L., Paquier, A., 2015. Alternate bar development in an alpine river following engineering works. *Adv. Water Resour.* 81, 103–113. <https://doi.org/10.1016/j.advwatres.2015.03.003>.
- Jansen, P., Van Bendegom, L., Van Den Berg, J., de Vries, M., Zanen, A., 1979. *Principles of River Engineering: The non-Tidal Alluvial River*. Pitman, London. Heruitgave Delftse Uitgevers Maatschappij, 1994 reprint, ISBN 90 6562 146 6.
- Kaless, G., Mao, L., Lenzi, M., 2014. Regime theories in gravel-bed rivers: models, controlling variables, and applications in disturbed Italian rivers. *Hydrol. Process.* 28 (4), 2348–2360. <https://doi.org/10.1002/hyp.9775>.
- Kennedy, R.G., 1895. The prevention of silting in irrigation canals. In: Paper presented at the The proceedings of the Institution of Civil Engineers, 119, pp. 281–290.
- Kleinhans, M.G., van den Berg, J.H.J.E.S.P., & Landforms. (2011). River channel and bar patterns explained and predicted by an empirical and a physics-based method. 36(6), 721–738. doi:<https://doi.org/10.1002/esp.2090>.
- Kleinhans, M.G., Braudrick, C., van Dijk, W.M., van de Lageweg, W.I., Teske, R., van Oorschot, M., 2015a. Swiftness of biomorphodynamics in Lilliput- to Giant-sized rivers and deltas. *Geomorphology* 244, 56–73. <https://doi.org/10.1016/j.geomorph.2015.04.022>.
- Kleinhans, M.G., van Scheltinga, R.T., van der Vegt, M., Markies, H., 2015b. Turning the tide: growth and dynamics of a tidal basin and inlet in experiments. *J. Geophys. Res. Earth Surf.* 120, 95–119. <https://doi.org/10.1002/2014JF003127>.
- Koch, F., Flokstra, C., 1980. In: *Bed Level Computations for Curved Alluvial Channels: Prepared for the 19th IAHR Congress*. Waterloopkundig Laboratorium, New Delhi, India, February 1981.
- Kondolf, G.M., Podolak, K., Grantham, T.E., 2013. Restoring mediterranean-climate rivers. *Hydrobiologia* 719 (1), 527–545. <https://doi.org/10.1007/s10750-012-1363-y>.
- Kondolf, G.M., Gao, Y., Annandale, G.W., Morris, G.L., Jiang, E., Zhang, J., Yang, C.T., 2014. Sustainable sediment management in reservoirs and regulated rivers: experiences from five continents. *Earth's Fut.* 2 (5), 256–280.
- Lacey, G., 1930. In: *Stable channels in alluvium Paper presented at the Minutes of the Proceedings of the Institution of Civil Engineers*, 229, pp. 259–292.
- Le, T., Crosato, A., Uijttewaal, W., 2018. Long-term morphological developments of river channels separated by a longitudinal training wall. *Adv. Water Resour.* 113, 73–85. <https://doi.org/10.1016/j.advwatres.2018.01.007>.
- Leopold, L.B., Maddock, T., 1953. *The Hydraulic Geometry of Stream Channels and Some Physiographic Implications*. US Government Printing Office (Vol. 252).
- Leopold, L.B., Wolman, M.G., 1957. In: *River channel patterns: Braided, meandering, and straight (282B)*. Washington, D.C. Retrieved from: <https://pubs.er.usgs.gov/publication/pp282B>.
- Limaye, A.B., 2020. How do braided rivers grow channel belts? *J. Geophys. Res.* 125, e2020JF005570 <https://doi.org/10.1029/2020JF005570>.
- Luppi, L., Rinaldi, M., Teruggi, L.B., Darby, S.E., Nardi, L., 2009. Monitoring and numerical modelling of riverbank erosion processes: a case study along the Cecina River (central Italy). *Earth Surf. Processes Landforms* 34 (4), 530–546. <https://doi.org/10.1002/esp.1754>.
- Meyer-Peter, E., Muller, R., 1948. *Formulas for Bed Load Transport*. Proceedings of 2nd meeting of the International Association for Hydraulic Structures Research. Delft 39–64.
- Jang, C.L., Shimizu, Y., 2005. Numerical simulation for braided rivers with erodible banks. *KSCE J. Civ. Eng.* 9 (429) <https://doi.org/10.1007/BF02830633>.
- Métivier, F., Lajeunesse, E., Devauchelle, O., 2017. Laboratory rivers: lacey's law, threshold theory, and channel stability. *Earth Surf. Dynam.* 5, 187–198. <https://doi.org/10.5194/esurf-5-187-2017>.
- Millar, R.G., 2005. Theoretical regime equations for mobile gravel-bed rivers with stable banks. *Geomorphology* 64 (3–4), 207–220. <https://doi.org/10.1016/j.geomorph.2004.07.001>.
- Mosselman, E., 2004. Hydraulic geometry of straight alluvial channels and the principle of least action. *J. Hydraul. Res.* 42 (2), 219–222. <https://doi.org/10.1080/00221686.2004.9728386>.
- Murray, A.B., Paola, C., 1994. A cellular model of braided rivers. *Nature* 371 (6492), 54–57.
- ONEMA (2018). Towards the restoration of rivers and aquatic environments. A collection of river hydromorphology restoration examples (<http://www.onema.fr/EN/EV/cat7a-rex2014.html>, last access 1 December 2018).
- Parker, G., 1978a. Self-formed straight rivers with equilibrium banks and mobile bed. Part 1. The sand-silt river. *J. Fluid Mech.* 89 (1), 109–125. <https://doi.org/10.1017/S0022112078002499>.
- Parker, G., 1978b. Self-formed straight rivers with equilibrium banks and mobile bed. Part 2. The gravel river. *J. Fluid Mech.* 89 (1), 127–146. <https://doi.org/10.1017/S0022112078002505>.
- Parker, G., 1979. Hydraulic geometry of active gravel rivers. *J. Hydraul. Div., ASCE* 105, 1185–1201 (HY9, Proc. Paper, 14841).
- Parker, G., Klingeman, P.C., Mclean, D.G., 1982. Bedload and size distribution in paved gravel-bed streams. *J. Hydraul. Eng.* 108 (HY4), 544–571.
- Parker, G., Toro-Escobar, C.M., Ramey, M., Beck, S., 2003. The effect of floodwater extraction on the morphology of mountain streams. *J. Hydraul. Eng.* 129, 885–895. [https://doi.org/10.1061/\(ASCE\)0733-9429\(2003\)129:11\(885\)](https://doi.org/10.1061/(ASCE)0733-9429(2003)129:11(885)).
- Parker, G., Wilcock, P.R., Paola, C., Dietrich, W.E., Pitlick, J., 2007. Physical basis for quasi-universal relations describing bankfull hydraulic geometry of single-thread gravel bed rivers. *J. Geophys. Res.* 112 (F4) <https://doi.org/10.1029/2006JF000549>.
- Pfeiffer, A.M., Finnegan, N.J., Willenbring, J.K., 2017. Sediment supply controls equilibrium channel geometry in gravel rivers. *Proc. Natl. Acad. Sci.* 114 (13), 3346–3351. <https://doi.org/10.1073/pnas.1612907114>.
- Pitlick, J., Marr, J., Pizzuto, J., 2013. Width adjustment in experimental gravel-bed channels in response to overbank flows. *J. Geophys. Res. Earth Surf.* 118, 553–570. <https://doi.org/10.1002/jgrf.20059>.
- Roelvink, J.A., 2006. Coastal morphodynamics evolution techniques. *Coastal Engineering* 53 (2-3). <https://doi.org/10.1016/j.coastaleng.2005.10.015>.
- Schmitt, K., Schäffer, M., Koop, J., Symmann, L., 2018. River bank stabilisation by bioengineering: potentials for ecological diversity. *J. Appl. Water Eng. Res.* 1–12.
- Schumm, S.A., Kahn, H.R., 1972. Experimental study of channel patterns. *Bulletin* 83, 1755–1770.
- Schuurman, F., Marra, W.A., Kleinhans, M.G., 2013. Physics-based modeling of large braided sand-bed rivers: bar pattern formation, dynamics, and sensitivity. *J. Geophys. Res.* 118 (4), 2509–2527. <https://doi.org/10.1002/2013JF002896>.

- Schuurman, F., Kleinhans, M.G., 2018. Response of braiding channel morphodynamics to peak discharge changes in the Upper Yellow River. *Earth Surf. Process. Landforms* 43, 1648–1662. <https://doi.org/10.1002/esp.4344>.
- Shields, A., 1936. Application of Similarity Principles and Turbulence Research to Bed-Load Movement. Hydrodynamics Laboratory Publication. No. 167, W. P. Ott and J. C. van Uchelen, trans., U.S. Dept. of Agriculture, Soil Conservation Service, Cooperative Laboratory, California Institute of Technology, Pasadena, Calif.
- Singh, U., 2015. Controls on and morphodynamic effects of width variations in bed-load dominated alluvial channels: Experimental and numerical study. PHD Thesis. University of Trento.
- Singh, U., Crosato, A., Giri, S., Hicks, M., 2017. Sediment heterogeneity and mobility in the morphodynamic modelling of gravel-bed braided rivers. *Adv. Water Resour.* 104, 127–144. <https://doi.org/10.1016/j.advwatres.2017.02.005>.
- Singh, V.P., 2003. On the theories of hydraulic geometry. *Int. J. Sediment Res.* 18 (3), 196–218.
- Stecca, G., Hicks, D.M., 2022. Numerical simulations of confined braided river morphodynamics: display of deterministic chaos and characterization through turbulence theory. *J. Geophys. Res.* 127, e2021JF006409 <https://doi.org/10.1029/2021JF006409>.
- Struiksma, N., Olesen, K., Flokstra, C., De Vriend, H., 1985. Bed deformation in curved alluvial channels. *J. Hydraul. Res.* 23 (1), 57–79. <https://doi.org/10.1080/00221688509499377>.
- Sun, J., Lin, B., Yang, H., 2015. Development and application of a braided river model with non-uniform sediment transport. *Adv. Water Resour.* 81, 62–74. <https://doi.org/10.1016/j.advwatres.2014.12.012>.
- Talmon, A., Struiksma, N., Van Mierlo, M., 1995. Laboratory measurements of the direction of sediment transport on transverse alluvial-bed slopes. *J. Hydraul. Res.* 33 (4), 495–517. <https://doi.org/10.1080/00221689509498657>.
- Teruggi, L., & Rinaldi, M. (2009). *Analysis of planimetric channel changes along the Cecina River (central Italy)*. Paper presented at the International proceedings of 27th IAS meeting of sedimentology. Medimond, Bologna, Italy.
- Tubino, M., Seminara, G., 1990. Free–forced interactions in developing meanders and suppression of free bars. *J. Fluid Mech.* 214, 131–159. <https://doi.org/10.1017/S0022112090000088>.
- Van Maanen, B., Coco, G., Bryan, K.R., 2013. Modelling the effects of tidal range and initial bathymetry on the morphological evolution of tidal embayments. *Geomorphology* 191, 23–34. <https://doi.org/10.1016/j.geomorph.2013.02.023>.
- Van Rijn, L.C., 1993. Principles of Sediment Transport in rivers, Estuaries and Coastal Seas. Aqua publications Amsterdam (Vol. 1006).
- Vargas-Luna, A., Crosato, A., Byishimo, P., Uijtewaal, W.S., 2019. Impact of flow variability and sediment characteristics on channel width evolution in laboratory streams. *J. Hydraul. Res.* 57 (1), 51–61. <https://doi.org/10.1080/00221686.2018.1434836>.
- Wickert, A.D., Martin, J.M., Tal, M., Kim, W., Sheets, B., Paola, C., 2013. River channel lateral mobility: metrics, time scales, and controls. *J. Geophys. Res. Earth Surf.* 118, 396–412. <https://doi.org/10.1029/2012JF002386>.
- Wilkerson, G.V., Parker, G., 2011. Physical Basis for Quasi-Universal Relationships Describing Bankfull Hydraulic Geometry of Sand-Bed Rivers. *J. Hydraul. Eng.* 137 (7), 739–753. [https://doi.org/10.1061/\(ASCE\)HY.1943-7900.0000352](https://doi.org/10.1061/(ASCE)HY.1943-7900.0000352).
- Williams, G., 1978. Bank-full discharge of rivers. *Water Resour. Res.* 14 (6), 1141–1154. <https://doi.org/10.1029/WR014i06p01141>.
- Williams, R., Measures, R., Hicks, D., Brasington, J., 2016. Assessment of a numerical model to reproduce event-scale erosion and deposition distributions in a braided river. *Water Resour. Res.* 52 (8), 6621–6642. <https://doi.org/10.1002/2015WR018491>.
- Van De Lageweg, W.I., Van Dijk, W.M., Kleinhans, M.G., 2013. Morphological and stratigraphical signature of floods in a braided gravel-bed river revealed from flume experiments. *J. Sediment. Res.* 83 (11), 1033–1046. <https://doi.org/10.2110/jsr.2013.70>.
- Wong, M., Parker, G., 2006. Reanalysis and correction of bed-load relation of Meyer-Peter and Müller using their own database. *J. Hydraul. Eng.* 132 (11), 1159–1168. [https://doi.org/10.1061/\(ASCE\)0733-9429\(2006\)132:11\(1159\)](https://doi.org/10.1061/(ASCE)0733-9429(2006)132:11(1159)).